Marte Thuen

Manganese-enhanced and diffusion tensor MR imaging of the normal, injured and regenerating rat visual pathway

Thesis for the degree of philosophiae doctor

Trondheim, July 2008

Norwegian University of
Science and Technology
Faculty of Medicine
Department of Circulation and Medical Imaging

NTNU
Norwegian University of
Science and Technology

NTNU
Norwegian University of Science and Technology

Thesis for the degree of philosophiae doctor

Faculty of Medicine
Department of Circulation and Medical Imaging

ISBN 978-82-471-7782-2 (printed ver.)
ISBN 978-82-471-7796-9 (electronic ver.)
ISSN 1503-8181

Theses at NTNU, 2008:90

Printed by Tapir Uttrykk

Doctoral theses at NTNU 2008:90

Marte Thuen

Manganese-enhanced and diffusion tensor MR imaging of the normal, injured and regenerating rat visual pathway

Norwegian University of Science and Technology
Department of Circulation and Medical Imaging
ISBN 978-82-471-7796-9 (electronic)
ISBN 978-82-471-7782-2 (printed)

NTNU
Innovation and Creativity

Manganforsterket og diffusjonstensor MR-avbildning av normal, skadet og regenererende synsnerve hos rotte

Sentralnervesystemet hos pattedyr regenererer ikke spontant etter nerveskade, og i dag finnes det ingen medisinsk behandling tilgjengelig i klinisk rutine. Dette gjør at pasienter med skader i sentralnervesystemet, for eksempel i ryggmargen, mest sannsynlig blir lam resten av livet.

Man har i den senere tid oppdaget at eksperimentelle behandlinger kan føre til noe regenerasjon i sentralnervesystemet. Men det er relativt lite regenerasjon som oppnås, så mer forskning må til før behandlingen kan føre til mer fullstendig regenerasjon og gjenvinning av funksjon for disse pasientene. For å teste de ulike eksperimentelle medikamentene og behandlingsformene er det vanlig å benytte seg av dyreforsøk hvor dyrene påføres en nerveskade, mottar behandling, for så bli avlivet. Deretter studeres sentralnervesystemet i histologiske snitt, og effekten av behandlingen evalueres. MR-avbildning (MRI) tillater avbildning av levende dyr. Muligheten for å studere skader i sentralnervesystemet flere ganger over tid, samt å evaluere effekten av diverse eksperimentelle behandlingsformer uten å måtte avlive dyrene først, vil være en stor fordel. Hovedformålet med denne avhandlingen er å utvikle MR-metoder som gjør dette mulig.

Paramagnetiske manganioner øker signalet i MR-bilder, og denne teknikken kalles manganforsterket MRI (MEMRI). Dessuten tas manganionene opp av nerveceller og transporteres langs nervebanene, noe som tillater spesifikk avbildning av nervebanene i sentralnervesystemet. På grunn av nervebanenes struktur, er diffusjon av vannmolekyler større langs enn på tvers av nervebanene. Diffusjonstensor avbildning (DTI) er en MR-teknikk hvor dette utnyttes til å avbilde nervebaner. I denne avhandlingen etableres det eksperimentelle teknikker hvor MEMRI og DTI benyttes for å studere sentralnervesystemet. Synsnerven hos rotte er valgt som eksperimentell modell. Den begynner like bak øyet, og aksonene, som danner synsnerven, går fra øyet og helt til bakre del av hjernen.

Hovedresultatene viser at både MEMRI og DTI tydelig viser nervebanene i normale synsnerver, og begge teknikkene kan benyttes for å detektere nerveskade i synsnerven. Videre viser resultatene at etter nerveskade og eksperimentell behan-

dling, vises økt signal i skadeområde etter tre uker, som tyder på at regenerasjon har funnet sted etter, og at dette kan detekteres ved hjelp av MR-avbildning. MR-undersøkelsen ble gjentatt flere ganger over tid for å følge utviklingen i sentralnervesystemet hos dyrene, noe som er unikt for MR sammenlignet med tradisjonelle histologiske metoder. Toksiske effekter av mangan ble evaluert, og det bli vist at mangan ikke er toksisk ved den dosen som er nødvendig for å oppnå tilstrekkelig kontrast i synsnerven på MR-bildene. Det ble dessuten vist at levende og velfungerende aksoner er et kriterium for å få mangantransport i nervene, noe som viser at mangan transporteres aktivt av aksonene.

Metodene som er utviklet i dette arbeidet gir ny kunnskap som kan benyttes i utvikling av nye medikamenter for regenerasjon i dyremodeller, samt bli verdifulle også i andre eksperimentelle dyremodeller. Samtidig er det et potensial for at metodene etter hvert også kan brukes i klinisk sammenheng. DTI er allerede på vei inn i klinikken, som et verktøy for å studere nervebaner i sentralnevesystemet hos mennesket. Likeledes, forutsatt at man løser problemene knyttet til toksisitet, kan man se for seg at MEMRI en gang i fremtiden kan bli et nyttig verktøy for å studere funksjonelle og strukturelle endringer i sentralnervesystemet.

Marte Thuen

Institutt for sirkulasjon og bildediagnostikk.
Veiledere: Olav Haraldseth og Christian Brekken.

Overnevnte avhandling er funnet verdig til å forsvares offentlig for graden Philosophiae Doctor i medisinsk teknologi.
Disputasen finner sted i Seminarrom, 1902-bygget, St. Olavs Hospital Tirsdag 26. august 2008 kl 12:15.

Acknowledgments

This thesis is the result of my work for the degree of Philosophiae Doctor, carried out at the FUGE Molecular Imaging Center, located at the MR center and part of Department Circulation and Medical Imaging, Faculty of Medicine, Norwegian University of Science and Technology (NTNU). Financial support was provided by the Faculty of Medicine, NTNU.

First of all, I would like to thank my supervisors Professor Olav Haraldseth and Dr Christian Brekken for initiating the projects and inviting me to participate, and for support and guidance throughout my PhD-period. Olav for always for seeing the big picture when everybody else is too focused on the details, and Christian for continuous advice and encouragement, as well as guidance in experimental planning, interpretation of results and many valuable, scientific discussions. Furthermore, I would like to thank Professor Martin Berry and Dr Axel Sandvig for being involved in the initiation of the project, helping with experimental planning, surgical procedures and guidance in writing the papers. I would also like to thank all co-authors of the papers included in this thesis. I am very grateful for all suggestions, critique and contributions.

Several colleagues at the MR-center have been involved in making this PhD possible. First of all, I would like to thank Tina Bugge Pedersen for helping with animal experiments and also for taking care of the little things. Furthermore, Christian Brekken, Anders Kristoffersen, Trond Singstad, Øystein Olsen and Pål Erik Goa for helping with optimizing of MRI sequences, solving practical MRI problems and developing data analyzing tools. Also, I would like to thank the staff at the Animal facility for taking care of my animals, and the Associate Professor Sverre Torp and technician Unn Granli at the Department of Laboratory Medicine, NTNU, for helping with histology.

A special thanks goes to all my colleagues at the MR-center for providing a positive working environment and making a my time here so wonderful. I would also like to thank friends and family for your continuous love and support. A special thanks goes to my dearest Håvard, for invaluable help in preparing this document in latex, but more importantly, for always being there. Last, but not least, I am forever grateful for my little boy Andre, who has made this last one and a half years so much more meaningful.

Marte Thuen,

Trondheim, April 2008

Summary

Central nervous system (CNS) axons do not regenerate spontaneously after injury, thus most patients with CNS injury face poor prognosis. Currently, there are no treatments available in routine clinical practice. However, it has been known since the 1980s that CNS axons can regenerate to some extent when supported with the appropriate experimental environment. Because of the extreme complexity of the molecular mechanisms governing the human CNS, the development of efficient treatments leading to neuronal regeneration in humans suffering from CNS injury seems difficult. Nevertheless, because of the dramatic impact such therapies will have on human healthcare, development of such therapies is a highly active field of research, and new drugs and treatments are constantly being tested in animal models. Usually, traditional tract tracing methods that requires sacrificing of the animals before tissue sectioning and analysis are used. Magnetic resonance imaging (MRI) is a non-invasive imaging modality, allowing longitudinal imaging. Sensitive MRI techniques for the monitoring of CNS injury and regeneration would constitute a major advancement that will benefit of a large patient population.

Manganese (Mn^{2+}) is paramagnetic and reduces the longitudinal relaxation time T_1, increasing tissue contrast in MR images. Additionally, Mn^{2+} is a calcium analogue that can be taken up by and transported along axons. This makes Mn^{2+} a unique contrast agent well suited for MRI of neural paths, a technique referred to as manganese-enhanced MRI (MEMRI).

Because of the longitudinal arrays of neurofilaments and microtubules in axons, as well as axonal membranes and myelin sheaths, the diffusion of water molecules along axons is greater that diffusion perpendicular to axons, and this is called anisotropic diffusion. In diffusion tensor imaging (DTI), a diffusion tensor that describes the water diffusion in all directions is generated, enabling non-invasive tracing of neural paths without the use of contrast agents.

In this PhD-thesis, methods for *in vivo* longitudinal MEMRI and DTI of the normal, injured and regenerating rat visual pathway were established. The rat visual pathway was chosen as an experimental model of the mammalian CNS. We have demonstrated that 3D MEMRI of the rat brain can be used longitudinally and Mn^{2+}-enhancement of the entire normal visual pathway was seen 24 h af-

ter intravitreal injection (150 nmol $MnCl_2$). After complete axonal injury of the optic nerve, no Mn^{2+}-enhancement was observed distal to the injury site, demonstrating that CNS injury can be detected using MEMRI. The clinically available Mn^{2+}-based contrast agent MnDPDP resulted in sufficient Mn^{2+}-contrast enhancement of the ON after $12 - 24$ h similar to that after $MnCl_2$-injection. In contrast, intravitreal Gd^{3+}-injection, resulted in enhancement of the vitreous only, and not in the retina or optic nerve, demonstrating the uniqueness of Mn^{2+} as a contrast agent. The highest Mn^{2+}-contrast enhancement of the visual pathway was seen after $150 - 300$ nmol $MnCl_2$. Higher doses were toxic, causing reduced Mn^{2+}-enhancement throughout the visual pathway because of retinal ganglion cell (RGC) death and subsequent loss of Mn^{2+}-transport in the axons. After $MnCl_2$-injection directly into the optic nerve, Mn^{2+}-enhancement was seen distal to the injection site, but no Mn^{2+}-enhancement was seen in the retina, indicating that Mn^{2+}-traffic is mainly mediated by anterograde transport. Intravitreal injections of 150 nmol $MnCl_2MnCl_2$ had a protective effect and saved more axons in retina in rats with optic nerve injury. DTI allowed for visualized of the normal optic nerve, and clearly detected optic nerve injury. Intravitreal peripheral nerve grafts (PNG) were used to stimulate regeneration after axonal injury of the optic nerve. At 21 day post lesion (dpl), an increase was observed in contrast to noise ratio (CNR) in MEMRI and axial diffusivity ($\lambda_{\|}$) in DTI at the injury site compared to that measured at 1dpl in rats with optic nerve injury and intravitreal PNG, indicating that axons have regenerated though the injury and beyond, and that this can be detected using MEMRI and DTI.

While MEMRI measures axonal function, DTI mainly reflects structural changes, and thus, MEMRI and DTI are complementary methods for imaging the normal, injured and regenerating axons in the visual pathway. The results of this thesis demonstrate the feasibility for MEMRI and DTI as tools for *in vivo*, longitudinal monitoring of CNS injury, and regeneration after therapeutic intervention.

Symbols and abbreviations

Ca^{2+}	calcium
α	flip angle
b	diffusion weighting factor
CNR	contrast to noise ratio
CNS	central nervous system
d	days
$\underline{\mathbf{D}}$	diffusion tensor
D	diffusion coefficient
dpl	days post lesion
FA	fractional anisotropy
FLASH	fast low-angle shot
Gd^{3+}	gadolinium
h	hour
λ_i	eigenvalue
$\lambda_\parallel$	axial diffusivity
$\lambda_\perp$	radial diffusivity
LGN	lateral geniculate nucleus
Mdiff	Mean diffusivity
MEMRI	manganese-enhanced MRI
min	minutes
$MnCl_2$	manganese chloride
MnDPDP	manganese dipyridoxyl diphosphate
MRI	magnetic resonance imaging

MR	magnetic resonance
ONC	optic nerve crush
ON	optic nerve
PNG	peripheral nerve graft
PNS	peripheral nervous system
RGC	retinal ganglion cells
ρ	proton density
ROI	region of interest
SC	superior colliculus
SD	standard deviation
s	seconds
SEM	standard error of the mean
SE	spin echo
S	signal
S_0	signal from non-enhanced tissue
S_{Mn}	signal from Mn^{2+}-enhanced tissue
SNR	signal to noise ratio
TE	echo time
T_1	longitudinal relaxation time
T_2	transversal relaxation time
TR	repetition time
Tr	Trace of a tensor

List of papers

Paper I
Manganese-enhanced MRI of the optic visual pathway and optic nerve injury in adult rats.
Marte Thuen, Trond E. Singstad, Tina Bugge Pedersen, Olav Haraldseth, Martin Berry, Axel Sandvig, and Christian Brekken.
Journal of Magnetic Resonance Imaging 22:492–500, 2005.

Paper II
Axon tracing in the adult rat optic nerve and tract after intravitreal injection of MnDPDP using a semi-automatic segmentation technique.
Øystein Olsen, Marte Thuen, Martin Berry, Vassili Kovalev, Maria Petrou, Pål Erik Goa, Axel Sandvig, Olav Haraldseth, and Christian Brekken.
Journal of Magnetic Resonance Imaging 27:34–42, 2008.

Paper III
Manganese-enhanced MRI of the rat visual pathway: acute neural toxicity, contrast enhancement, axon resolution, axonal transport and clearance of Mn^{2+}.
Marte Thuen, Martin Berry, Tina Bugge Pedersen, Pål Erik Goa, Mike Summerfield, Olav Haraldseth, Axel Sandvig, and Christian Brekken.
In press. To be published in Journal of Magnetic Resonance Imaging.

Paper IV
Combination of Mn^{2+}-enhanced and diffusion tensor MR imaging gives complementary information about injury and regeneration in the adult rat optic nerve.
Marte Thuen, Øystein Olsen, Martin Berry, Tina Bugge Pedersen, Anders Kristoffersen, Olav Haraldseth, Axel Sandvig, and Christian Brekken.
Accepted for publication in Journal of Magnetic Resonance Imaging.

Contents

Chapter 1

Introduction

1.1 Clinical background

Axons in the central nervous system (CNS) of adult mammals do not regenerate spontaneously after injury, thus, CNS injury will often result in paralysis and permanent loss of function. CNS damage occurs in neurodegenerative diseases such as multiple sclerosis (MS), Alzheimer's disease and Parkinson's disease and in traumatic injuries such as brain trauma, stroke and spinal cord injury. All of these are conditions in which there currently are few clinical treatments available and thus little or no hope of recovery.

That the adult mammalian CNS is incapable of spontaneous regeneration was first documented by Ramon y Cajal in 1928 [94]. In contrast, axons in the CNS grow during development, and injured axons in the peripheral nervous system (PNS) have the ability to regenerate after injury [50, 54]. Furthermore, in non-mammalian vertebrates, such as fish and amphibian, regeneration after injury is seen both in the PNS and CNS [60]. The reasons for these differences are not known.

It was once believed that the adult CNS lacked any ability to regenerate after injury, however, in 1981, David and Aguayo demonstrated regeneration in the adult mammalian CNS after implantation of PNS fragments in the injury site [38]. This laid the route for a series of studies demonstrating CNS axonal regeneration after a variety of therapeutic strategies, and it is now well documented that CNS axons can regenerate when given the appropriate stimulation. In spite of this research effort, the degree of regeneration is low, and functional recovery is usually not achieved. Because of the major significance the regain of function after CNS injury will have on human health, and the promising findings of regeneration so far, this is a highly active research field. Currently, there are no treatments available for routine applications in clinical practice [93], but new therapeutic strategies and drugs are constantly being tested in animal models and clinical

trials around the world [112]. This gives great hope for current and future patients suffering from CNS injury and disease.

So far, most studies of regeneration in the CNS and the testing of therapeutic interventions have been carried out in animals using traditional axon tracing techniques [85, 86, 95, 107]. However, such post mortem techniques are not applicable to longitudinal studies of live animals. The ability to perform *in vivo* serial imaging for studying the process of regeneration in the CNS would constitute a major advantage.

MRI offers the potential for non-invasive, longitudinal monitoring of animals. In this thesis, methods for *in vivo* longitudinal manganese-enhanced MRI (MEMRI) and diffusion tensor imaging (DTI) are established, with the purpose of studying the normal, injured and regenerating adult rat visual pathway. The results show that both MEMRI and DTI are promising tools that can be used in the development and testing of new therapeutics that stimulate regeneration in the CNS.

In addition to being tools for monitoring the effect of therapeutic interventions on regeneration in animals, DTI and MEMRI have potentials for being used in clinical diagnostics of CNS injury and response to treatment. DTI is currently being introduced in clinical MR imaging, for example in pre-surgical planning of patients with brain tumors. Introduction of MEMRI of the CNS into the clinic is not equally straightforward, especially because of Mn^{2+}-toxicity. However, given that the limitations of MEMRI could be overcome, MEMRI might become a sensitive method for detecting functional changes in CNS injury and regeneration, giving complementary information to DTI.

1.2 Axonal damage and regeneration in the central nervous system

In the PNS, injured axons will regenerate after injury. Schwann cells in the PNS produce myelin and neurotrophic factors to support axonal regeneration. Additionally, the lesion cavity is filled with a permissive matrix of collagen, fibronectin, laminin and fibroblasts that support axonal growth, and genes that promotes axonal regeneration are activated in the injured PNS neurons [73]. In the CNS, the situation is quite different. When an axon is cut, the distal segment of the axons is isolated from its cell body. Within few days after injury, the axon undergoes Wallerian degradation and die [15]. The proximal part of the axon survives to a greater degree [54], but will not regenerate spontaneously [40, 94]. Myelin-associated inhibitory molecules, such as myelin-associated glycoprotein (MAG)

and Nogo-A are present in the CNS, preventing axonal regeneration after injury [39, 76, 101]. Immediately after CNS injury, the formation of a glial scar starts. In addition to being a physical barrier for regenerating axons, several growth inhibitory molecules, such as for example chondroitin sulfate proteoglycans, are preset in the scar, hindering axonal growth [39]. Furthermore, the absence of growth-promoting neurotrophic factors in the CNS prevents spontaneous regeneration [19].

The molecular mechanisms involved in the response to injury and those that regulate the lack of CNS regeneration are very complex. Thus, there are numerous possible ways for scientists to interfere with the molecular mechanisms in the hopes of inducing regeneration in the CNS. One strategy has been to try neutralizing the myelin inhibitory molecules and degrade the inhibitory components of the glial scar. The bacterial enzyme chondroitinase ABC degrades the glial scar and create a more permissive environment for axonal regeneration [28, 78]. Another way is to administer growth-promoting molecules, which make the lesion environment less hostile to growth. Implantation of a peripheral nerve graft (PNG) in the proximity of the lesion will generate a release of growth factors from the Schwann cells in the graft. This will enable the CNS axons to mount a more vigorous regenerative axonal-growth program and can promote regeneration in the CNS [20, 47, 54, 64, 114]. A promising technique is use of olfactory ensheathing cells (OEC). These glial cells are found in the olfactory system, where they accompany the olfactory axons into the CNS. This is the only place in the adult mammalian CNS where regeneration can, in fact, occur [92]. OEC can be transplanted into the CNS lesion area, where they encourage axonal growth [68, 69]. Several groups have shown that stem cell therapy can be used to promote functional recovery after CNS injury in animal models. This include various types of stem cells such as bone marrow-derived stromal cells and adult neural precursor cells. After implantation, these stem cells migrate to the site of injury, where they can differentiate into oligodendrocytes, astrocytes and occasionally neurons, affecting the inhibitory environment of the injury site so that more of the spared axons are kept alive and also possible promoting regeneration of the injured axons [33, 87, 59, 113]. Combinations of the various techniques, such as Schwann cell bridges and olfactory ensheathing cells with chondroitinase can be especially beneficial for inducing regeneration [46]. Even though some recovery of function has been reported in these studies, the amount of regenerating axons is low. Thus, more research is needed in the quest of finding methods that can result in regeneration and permanent regain of function after CNS injuries.

1.3 The rat visual pathway

The axonal projections of retinal ganglion cells (RGC) constitute the visual pathway (Figure 1.1). RGC are located in the innermost layer of the retina and their axons form the optic nerve (ON) on leaving the eye at the lamina cribrosa. The rat optic nerve is approximately 9 mm long, 0.6 mm in diameter and contains about 120 000 axons [30, 31]. In rodents, the majority of RGC axons in the ON decussate in the optic chiasm and project into the contralateral optic tract to subcortical targets, including the thalamic lateral geniculate nucleus (LGN), midbrain pretectum, and superior colliculus (SC) [54, 121]. The pretectum is involved in the control of pupillary reflexes in response to light stimulation, as well as in the accommodation reflex. The SC is involved in the coordination of head and eye movements, and the LGN processes visual information before relaying it in the optic radiation to layer IV in the primary visual cortex where further processing occurs, resulting in visual perception [91, 119, 121].

1.4 Manganese-enhanced MRI

1.4.1 Mn^{2+} as a contrast agent

Paramagnetic substances, such as for example Gd^{3+}, Fe^{3+}, Cu^{2+} and Mn^{2+}, have unpaired electrons in their atoms, resulting in a small magnetic moment. In the absence of an external magnetic field, these magnetic moments are randomly distributed, and will thus cancel each other out. When an external magnetic field is applied, the magnetic moments will align with the direction of the applied field, producing an increase in the local magnetic field. The protons in the tissue will interact with the paramagnetic substances through dipole–dipole interactions, creating fluctuations in the magnetic field. This can affect both the longitudinal relaxation time T_1 and transversal relaxation time T_2 of the protons, and result in increased tissue contrast (in T_1-weighted images) or reduced tissue contrast (in T_2-weighted images) in the regions where the paramagnetic substances are present [51, 77].

Mn^{2+} was one of the first MRI contrast agent, used in the earliest stages of MRI [66, 67], and is mainly a T_1 contrast agent. In pure water, the relaxation rates are linearly dependent on the concentration of the paramagnetic substances [65]. *In vivo*, Mn^{2+} can bind to a variety of structures such as proteins and nucleic acids, and this strongly influence the magnetic properties in the surrounding tissue, leading to a reduction in T_1 and increased tissue contrast in T_1-weighted imaging [58, 84].

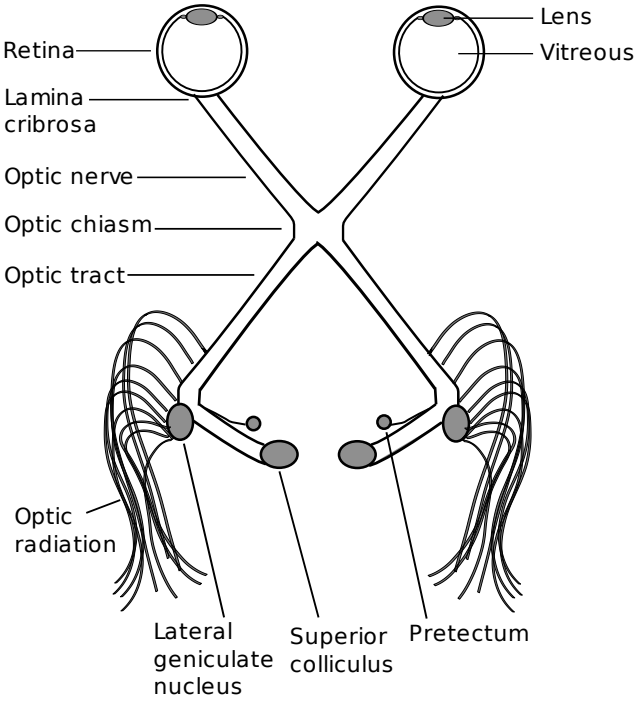

Figure 1.1: Illustration of the rat visual pathway. From the retina, axons project through the optic nerve (ON) and contralateral optic tract to lateral geniculate nucleus (LGN), the pretectum and the superior colliculus (SC). From the LGN, visual information is transferred via synaptic connections through the optic radiation to layer IV of the visual cortex.

Mn^{2+} is an essential trace metal, and is a co-factor in several biological processes [7]. The divalent cation Mn^{2+} is a calcium (Ca^{2+}) analogue and can enter cells through voltage gated Ca^{2+}-channels and other Ca^{2+}-transport systems [37, 83, 82, 88]. The simplest way for administration of Mn^{2+} is to use a $MnCl_2$-solution. In animals, $MnCl_2$ can be injected intravenously, subcutaneously, intraperitoneally or as an injection directly into the area of interest, if feasible, such as into the vitreous body of the eye. After injection, the salt dissolves into Mn^{2+} and Cl^{2-}. Mn^{2+} will enter cells through the Ca^{2+}-channels and react with and bind to intracellular components. How Mn^{2+} is distributed inside the cells is not known in detail.

Teslascan™ (GE Healthcare AS, Oslo, Norway) is the only commercially available Mn^{2+}-containing contrast agent. Teslascan consists of manganese dipyridoxyl diphosphate (MnDPDP), a chelated Mn^{2+}-compound, and is clinically approved for MRI of the human liver. MnDPDP contains two vitamin B6 parts that through nitrogen and oxygen bonds keep Mn^{2+} in a chelate that is highly soluble and stable in pure water [96]. *In vivo*, for example after intravenous administration, MnDPDP is metabolized to manganese dipyridoxyl monophosphate (MnDPMP) and manganese dipyridoxyl ethylendiamine diacetate (MnPLED). The MnDPDP and MnPLED metabolites are simultaneously trans-metaled with zinc (Zn^{2+}), releasing Mn^{2+} [118].

1.4.2 T_1-weighted MR-imaging

Mn^{2+} is mainly a T_1-agent, and MRI can be obtained using a T_1-weighted imaging sequence, for example a fast low flip angle shot (FLASH) sequence. FLASH is a short-TR steady-state incoherent gradient echo sequence that provides rapid image acquisition [51]. It uses small flip angle excitations combined with spoiling of transverse magnetization before the next RF pulse. In steady-state, the signal from a spoiled gradient echo sequence is gives by

$$S = \rho \sin\alpha \frac{1 - e^{-\frac{TR}{T_1}}}{1 - e^{-\frac{TR}{T_1}} \cos\alpha} e^{-\frac{TE}{T_{2*}}} \tag{1.1}$$

where ρ is the proton density, α is the flip angle, TR is the repetition time, TE is the echo time and T_1 and T_2 are the longitudinal and transversal relaxation times, respectively.

T_1-mapping gives the true T_1-values in each voxel of the tissue [34, 52], and is currently getting introduced as an alternative to T_1-weighted imaging . T_1-mapping can be more sensitive to changes in T_1 than T_1-weighted imaging, but

it is also more challenging with regards to obtaining good image quality as well as post processing.

1.4.3 Applications of MEMRI

Mn^{2+} can enter excited cardiac cells after systemic injection, accumulating in activated areas, and can be used in MR imaging of the heart. This has been demonstrated since the 1980s using $MnCl_2$ in animal models [77, 125] and also recently in the human heart after intravenous administration of a clinically safe dose of Teslascan [103]. Furthermore, MEMRI can separate viable and non-viable myocardium, and is a promising tool for detection of infarcted regions in both animal and human hearts [25, 102].

After systemic injection of $MnCl_2$, Mn^{2+} can enter the brain [63], and the transport of Mn^{2+} will be more efficient if the blood-brain barrier is disruption [8]. Mn^{2+} can act as a general contrast agent after systemic administration, enhancing soft tissue contrast [4], however, as for the heart, the uptake of Mn^{2+} is more efficient in activated neurons. Thus, Mn^{2+} will accumulate in activated areas of the brain, and MEMRI can be used to investigate such areas after an external stimulation (e.g. stimulation of the whiskers or fore paw on one side) [3, 126]. Since Ca^{2+} is one of the most robust indicators of neuronal activity [42], MEMRI will be a measure of brain activity. Furthermore, MEMRI can detect brain ischemia [2].

In 1995, Tjälve and coworkers demonstrated that radioactive Mn^{2+} was transported from the olfactory receptor neurons to the olfactory bulb in fish [117], and later confirming their findings in the rat olfactory pathway [116]. This demonstrates that Mn^{2+} is not only taken up by neurons, but is also transported along the axons. These studies were carried out *ex vivo* using γ-spectrometry and autoradiography. In 1998, Pautler and colleagues utilized the paramagnetic properties of Mn^{2+}, performing the first *in vivo* Mn^{2+}-tract tracing experiment [90]. They showed that after administration of $MnCl_2$ into the rat olfactory receptor neurons, contrast enhancement was seen in the olfactory bulb and primary olfactory cortex in MRI. Since this first experiment, MEMRI has been used to trace several pathways of the animal brain, including the visual, olfactory and hippocampal pathways, and the basal ganglia in rats, mice and monkeys [88, 100, 123, 124], as well as the song center in birds [70].

The mechanisms by which Mn^{2+} is transported along the axons are not known in detail. It is believed that an active transport mechanism is the main contributor to Mn^{2+}-traffic within the axons, however, passive diffusion can also contribute to the net Mn^{2+}-transport [89]. Administration of the microtubule disrupting

agent colchicine prior to Mn^{2+}-application lead to a reduced transport of Mn^{2+}, indicating that microtubule is involved in the Mn^{2+}-transport [88, 104]. The direction of Mn^{2+}-transport is mainly anterograde [104], and Mn^{2+} is transported at a rate of approximately $2-5$ mm/h [13, 90]. When the Mn^{2+}-ions reach the nerve endings, they are released into the synaptic cleft, where the may transverse the postsynaptic membrane through voltage-gated Ca^{2+}-channels [100, 111]. The transport of Mn^{2+} can carry on through the next nerve fiber, and may thus enhance structures far from the site of injection, for example the visual cortex after intravitreal injection [71]. After injection, the MRI signal is enhanced for several hours or days, depending on the dose of $MnCl_2$, area of interest and method of administration [63, 123].

These properties make Mn^{2+} a unique contrast agent well suited for tracing axonal pathways and neuronal connections in the CNS. Longitudinal studies are feasible, and tract tracing using MEMRI has the potential to be used in studies of CNS damage and repair.

1.4.4 Toxicity of manganese

Mn^{2+} is an essential metal found in a variety of biological tissue, and is necessary for normal functioning of several physiological processes [7]. Nevertheless, overexposure causes toxic reactions, and the toxicity of Mn^{2+} in the CNS is well documented [7, 36, 97]. In humans, long term exposure to Mn^{2+} induces Parkinsonian symptoms, including headaches, memory loss, emotional instability, rigidity, tremors, seizures and death [7, 36], and animal studies have shown neuronal degeneration after $MnCl_2$ injections into the striatum [26]. In the general population, Mn^{2+}-exposure is rarely a problem. The primary source of Mn^{2+}-poisoning is occupational exposure experienced by welders, miners, and workers in dry-cell battery factories and ferromanganese alloy plants [11, 24, 53, 55, 56, 57, 81]. The molecular mechanisms by which Mn^{2+} causes neurotoxicity is not known in detail, but it is believed that the basal ganglia nuclei are primary targets for Mn^{2+}-neurotoxicity [57, 9]. The experimental set up in MEMRI is usually different from the occupational exposure described above in regards to the applied dose of Mn^{2+}, way of administration, and the length of investigation. High concentrations of Mn^{2+} may inactivate voltage gated Ca^{2+} channels leading to unrestrained Ca^{2+} entry [29, 83]. Furthermore, Mn^{2+} might accumulate in mitochondria, which can lead to inhibition of electron transfer [130]. Additionally, Mn^{2+} can increase the production of reactive oxygen species which can lead to apoptosis of neurons [41, 131].

1.5 Diffusion tensor imaging

Diffusion tensor imaging (DTI) was introduced in the mid 1990s, when Basser and coworkers demonstrated that the direction of the Brownian motion of water molecules in tissue could be used to create contrast in MRI [12]. In pure liquid with no barriers, the diffusion of protons will be equal in all directions, and this is called isotropic diffusion. In uniform cellular tissue there can be barriers resulting in an isotropic diffusion with a reduced diffusion length. In some tissue types, such as muscles, myocardium and neurons, the barriers within the cells are oriented mainly in one direction, causing a higher degree of diffusion along these barriers compared to perpendicular to them. This is called anisotropic diffusion [14]. Neurons consist of bundles of axons which are often myelinated, and within each axons, there are longitudinal structures such as mictotubule and neurofilaments, which makes the diffusion of protons within neurons highly anisotropic (Figure 1.2 and 1.3). In the brain, the water diffusion in gray matter is isotropic, while that of normal white matter is anisotropic [80].

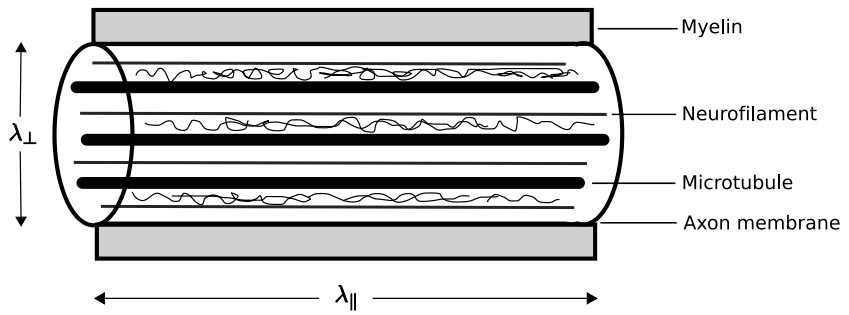

Figure 1.2: Illustration of anisotropic diffusion. In CNS white matter tracts, barriers within the cells, such as neurofilaments and microtubule, as well as myelin sheaths and cell membranes, are oriented mainly in one direction, leading to a higher degree of water diffusion in this direction, which is called anisotropic diffusion. Axial diffusivity ($\lambda_\parallel$) is defined as the magnitude of the water diffusion parallel to the axon. Radial diffusivity ($\lambda_\perp$) is defined as the magnitude of water molecules diffusion perpendicular to the axon.

To generate MR image based on the physical properties of water molecules, parameter such as proton density ρ, the relaxation times T_1 and T_2 and the diffusion

coefficient D are used. A simplified equation describing how these parameters contribute to the MR signal (S) in a spin-echo image is given as

$$S = \rho(1 - \mathrm{e}^{-\frac{\mathrm{TR}}{T_1}})\mathrm{e}^{-\frac{\mathrm{TE}}{T_2}}\mathrm{e}^{-\mathrm{b}D} = S_0\mathrm{e}^{-\mathrm{b}D} \tag{1.2}$$

where TR is the repetition time and TE is the echo time, defining the excitation and preparation times of the MR-sequence, and b is the diffusion weighting factor [79]. While ρ, T_1, T_2 and D are tissue specific parameters, TR, TE and b can be manipulated by the user. If two images with different b-values are obtained, keeping all other parameters constant, the diffusion coefficient D can be calculated from

$$S_1 = S_0\mathrm{e}^{-\mathrm{b}_1 D} \tag{1.3}$$

$$S_2 = S_0\mathrm{e}^{-\mathrm{b}_2 D} \tag{1.4}$$

$$\frac{S_2}{S_1} = \mathrm{e}^{-(\mathrm{b}_2 - \mathrm{b}_1)D} \tag{1.5}$$

$$D = -\frac{\ln\frac{S_2}{S_1}}{\mathrm{b}_2 - \mathrm{b}_1} \tag{1.6}$$

In the presence of anisotropy, the diffusion varies according to the direction, and can no longer be characterized by the scalar coefficient in (1.6). Thus, this requires the introduction of the diffusion tensor $\underline{\mathbf{D}}$, which fully describe the direction of the diffusion in all directions and the correlation between these directions in each voxel of the data volume [22]

$$\underline{\mathbf{D}} = \begin{bmatrix} D_{xx} & D_{xy} & D_{xz} \\ D_{yx} & D_{yy} & D_{yz} \\ D_{zx} & D_{zy} & D_{zz} \end{bmatrix} \tag{1.7}$$

Several parameters derived from the diffusion tensor can be used to describe the DTI data [22]. The *mean diffusivity* (Mdiff) describes the overall mean-squared displacement of the molecules, and the overall presence of obstacles, and is given by

$$\mathrm{Mdiff} = \frac{\mathrm{Tr}(\underline{\mathbf{D}})}{3} = \frac{D_{xx} + D_{yy} + D_{zz}}{3} \tag{1.8}$$

where Tr is the trace of the tensor. Because the diffusion tensor is symmetric and positive definite (has positive eigenvalues), it is diagonalizable, and the sum of the eigenvalues is equal to the trace. Thus, equation (1.8) can also be written as

$$\mathrm{Mdiff} = \frac{\lambda_1 + \lambda_2 + \lambda_3}{3} \tag{1.9}$$

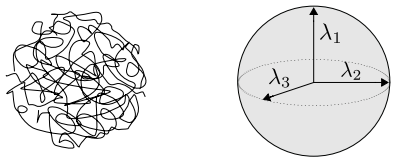

(a) Free, isotropic diffusion in liquid.

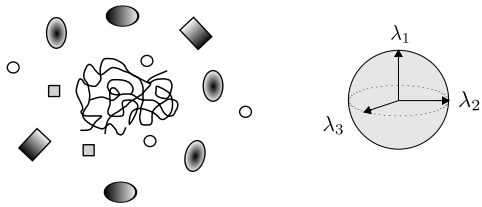

(b) Restricted, isotropic diffusion in uniform, cellular tissue.

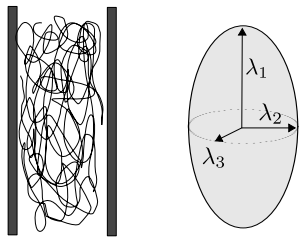

(c) Anisotropic diffusion in an axon.

Figure 1.3: Illustrations of (a) free isotropic, b) restricted isotropic and (c) anisotropic molecular water diffusion. The displacement of the water molecules forms an ellipsoid where the axis of the ellipsoid represent the eigenvalues of the diffusion tensor. For isotropic diffusion, $\lambda_1 = \lambda_2 = \lambda_3$ (with smaller values of λ in restricted isotropic diffusion (b)), while for anisotropic diffusion, $\lambda_1 > \lambda_2 = \lambda_3$.

The diffusion in each voxel can be illustrated as an ellipsoid (Figure 1.3), where the eigenvalues of the tensor represents the axis of the ellipsoid, and the shape of the ellipsoid describes the amount of anisotropic diffusion.

Fractional anisotropy (FA) is the degree of anisotropy, and characterizes how much molecular displacement varies in space due to the presence of oriented structures. FA is given as

$$\mathrm{FA} = \sqrt{\frac{1}{2}}\frac{\sqrt{(\lambda_1-\lambda_2)^2+(\lambda_2-\lambda_3)^2+(\lambda_3-\lambda_1)^2}}{\sqrt{\lambda_1^2+\lambda_2^2+\lambda_3^2}} \tag{1.10}$$

alternatively written as

$$\mathrm{FA} = \sqrt{\frac{3}{2}}\sqrt{\frac{(\lambda_1-\langle\lambda\rangle)^2+(\lambda_2-\langle\lambda\rangle)^2+(\lambda_3-\langle\lambda\rangle)^2}{\lambda_1^2+\lambda_2^2+\lambda_3^2}} \tag{1.11}$$

with $\langle\lambda\rangle = (\lambda_1+\lambda_2+\lambda_3)/3$.

The eigenvalues (λ_1, λ_2 and λ_3) derived from the diffusion tensor matrix diagonalization can be separated into components parallel (λ_1) and perpendicular (λ_2 and λ_3) to the axonal tract [106]. The axial diffusivity

$$\lambda_{\parallel} = \lambda_1 \tag{1.12}$$

is defined as the magnitude of the water diffusion parallel to the tract within the voxel of interest (Figure 1.2). The radial diffusivity

$$\lambda_{\perp} = \frac{\lambda_2+\lambda_3}{2} \tag{1.13}$$

is defines as the average magnitude of water molecules diffusion perpendicular to the tract.

DTI is a completely non-invasive MR imaging technique that is currently being introduced in clinical brain and spinal cord MRI. As axonal injury and other white matter pathologies would expect to affect the diffusion of water within the axons, DTI can be used to investigate such injuries. Furthermore, because DTI can visualize axonal tracts and neural connections in the human brain, it is a valuable technique for example in pre-surgical planning of patients with brain tumors.

Chapter 2

Aims of study

The main objective of this thesis was to develop and optimize techniques for MR imaging of the rat visual pathway for the purpose of establishing methods for longitudinal *in vivo* studies of ON injury and axonal regeneration in the visual pathway.

More specifically, the aims of this thesis were:

- to use MEMRI for studying the normal rat visual pathway *in vivo* and provide dose- and time-responses of Mn^{2+}-enhancement (Paper I).
- to investigate if MEMRI could be used to detect mechanically induced ON-injury (Paper I).
- to define MEMRI as a longitudinal tool for studying the normal and injured ON (Paper I).
- to study the similarities and differences between MnDPDP and $MnCl_2$ as contrast agents for MEMRI of the rat visual pathway, and compare them to the extracellular contrast agent gadodiamide (Paper II).
- to provide dose response data for safe and efficient use of $MnCl_2$ as a contrast agent for MEMRI of the rat visual pathway by studying RGC survival in retina and Mn^{2+}-contrast enhancement in the visual pathway with increasing doses of intravitreal $MnCl_2$ (Paper III).
- to study the relationship between MEMRI contrast enhancement and the dose of $MnCl_2$ and the number of surviving RGC (Paper III).
- to investigate the mode of axonal transport of Mn^{2+} and clearance of Mn^{2+} from the site of injection (Paper III).
- to investigate the potential for MEMRI as a tool for detecting regeneration after mechanically induced ON-injury and PNG implantation (Paper IV).

- to implement a DTI protocol for *in vivo* imaging of the rat ON that could be used in combination with MEMRI (Paper IV).
- to investigate the potential for DTI as a tool for detecting regeneration after mechanically induced ON-injury and intravitreal PNG implantation (Paper IV).

Chapter 3

Materials and Methods

3.1 Experimental setup

3.1.1 Experimental overview

An overview of the experiments performed in this thesis is presented in Table 3.1.

3.1.2 Animal handling

Inbred Fischer and outbred Sprague Dawley rats were used in these studies. The use of an inbred rat stain was necessary for successful implantation of intvavitreal PNG without causing immunological responses. Guidelines approved by the local ethical committee for animal research were followed and all experiments were approved by the responsible governmental authorities.

Rats were anesthetized during all Mn^{2+}-injections, surgical procedures and MR-experiments using either subcutaneous injections or isoflurane gas anesthesia. After experimental procedures, analgesia was provided if required.

In Papers I and II, subcutaneous injections of a 1:1:2 mixture of Hypnorm/Dormicum/sterile water (2.5 ml/kg), under sedation using 4% isoflurane in 3% O_2 was used for all experiments, including Mn^{2+}-injections, ONC and MEMRI.

In Paper III, subcutaneous injections of a 2:3:3:4 mixture of Haldol/Midazolam/Fentanyl/sterile water (4 ml/kg), under sedation using 4% isoflurane in 3% O_2 was used for MEMRI including Mn^{2+}-injections. For RGC counts, rats were prepared for anesthesia with a subcutaneous injection of Buprenorphine (0.03 mg/kg) and sedated throughout surgery with 4% isoflurane in 3% O_2.

In Paper IV, subcutaneous injections of a 2:3:3:4 mixture of Haldol/Midazolam/Fentanyl/sterile water (4 ml/kg), under sedation using 4% isoflurane in 3% O_2 was used for ONC, intravitreal PNG implantations and $MnCl_2$-injections. For

Table 3.1: Overview of the experiments in this thesis. In this thesis, the normal and injured ON were studied using MEMRI, DTI and histological methods. Several experiments were performed using these technique, which resulted in a total of 4 papers.

Normal ON	MEMRI	Longitudinal 1 d + 21 d	2.35 T	Paper I
		Dose-response/CNR $0.2 - 200$ nmol $MnCl_2$	2.35 T	
		Time-response $24 - 168$ h	2.35 T	
		$MnCl_2$, MnDPDP and Gd^{3+}	2.35 T	Paper II
		Mode of axonal transport	2.35 T	Paper III
		Dose-response/CNR $0 - 3000$ nmol $MnCl_2$	7 T	
	Histology (retina)	RGC-survival, $0 - 3000$ nmol $MnCl_2$		
	DTI	Longitudinal 1 d, 7 d, 14 d and 21 d	7 T	Paper IV
		Mn^{2+}-effect on DTI?	7 T	
Injured ON	MEMRI	ONC 1 d + 21 d	2.35 T	Paper I
		ONC + PNG 1 d + 21 d	7 T	Paper IV
	DTI	ONC + PNG 1 d + 21 d	7 T	
	Histology (retina)	ONC $\pm$ PNG 1 d + 21 d		
	Histology (ON)	ONC + PNG 21 d		

MEMRI and DTI, a 1:1:2 mixture of Hypnorm/Dormicum/ sterile water subcutaneously (2.5 ml/kg), under sedation using 4% isoflurane in 3% O_2 was used. For RGC counts, rats were prepared for anesthesia with a subcutaneous injection of Buprenorphine (0.03 mg/kg) and sedated throughout surgery with 4% isoflurane in 3% O_2.

After surgical procedures, post-surgical analgesia was controlled with subcutaneous injection of Buprenorphine (1.7 ml/kg in 1:10 sterile water). During MRI, eyes were smeared with Simplex lubricant to counteract corneal dehydration. Animals were kept in a pathological free environment at St. Olav's Hospital Animal Facility, with free access to food and water. Before MRI, animals were transported to the MR center in appropriate cages. During Mn^{2+}-injections

and surgical procedures (ONC and PNG implantations), anesthetized rats were placed in a custom designed head holder that could be rotated for optimal user interaction (Figure 3.1). During MRI, anesthetized rats lay prone in dedicated

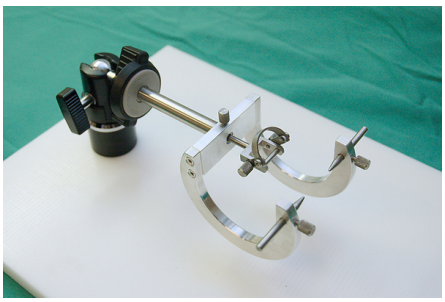

Figure 3.1: During Mn^{2+}-injections, ONC and intravitreal PNG implantations, anesthetized rats were placed in a custom designed rat head holder, which could be rotated for optimal user interaction.

animal bed within the magnet, heated with either circulating air (Papers I and II) or circulating water (Papers III and IV) to maintain a body temperature of 37 °C. The animal bed was designed to minimize animal movement, with a tooth bar, ear pins, tight space for the head and brackets for the surface coil.

3.1.3 $MnCl_2$-injections

$MnCl_2$-solutions were prepared by mixing the required amount of 1M $MnCl_2$-solution (Sigma-Aldrich Co, Steinheim, Germany) and sterile H_2O to obtain the appropriate dose of $MnCl_2$. An overview of the injections used in this thesis is shown in table 3.2. Using a purpose-built injection device consisting of a plastic syringe connected via polyethylene tubing to a glass micropipette with a tip diameter of $\sim$ 50 µm, aqueous $MnCl_2$ was injected into the vitreous body of anaesthetised rats, immediately posterior to the ora serrata of the left eye. After the injection, the pipette was slowly withdrawn to minimize reflux.

Direct injection into the ON : after accessing the intraorbital ON as described for optic nerve crush (ONC) (see below), 2 µl of aqueous $MnCl_2$ were administrated directly into the ON, approximatly 2 mm from the lamina cribrosa, using the injection device as described above.

Table 3.2: Overview of intravitreal injections used for MEMRI in this thesis. All injections were done intravitrally, except for the direct injection in Paper III, as indicated in the table.

	Solution	Amount	Concentration	Dose
Paper I	$MnCl_2$	3 µl*	50 mM	150 nmol
Paper II	$MnCl_2$	2 µl	100 mM	200 nmol
	MnDPDP	3 µl	10 mM	30 nmol
	gadodiamide	3 µl	500 mM	1500 nmol
Paper III	$MnCl_2$	3 µl	0 mM	0 nmol
		3 µl	10 mM	30 nmol
		3 µl	50 mM	150 nmol
		3 µl	100 mM	300 nmol
		3 µl	500 mM	1500 nmol
		3 µl	1000 mM	3000 nmol
	$MnCl_2$, direct inj.	2 µl	100 mM	200 nmol
Paper IV	$MnCl_2$	3 µl	50 mM	150 nmol

* In the dose-response experiment of Paper I, rats were given 2 µl of 0.1, 1, 2, 5, 7.5, 10, 25, 50, 75 or 100 mM $MnCl_2$.

3.1.4 Optic nerve crush and peripheral nerve graft implantation

Optic nerve crush (ONC) was performed according to the method described by Berry et al [19]. In brief, the dural sheath of the ON was incised longitudinally after intraorbital exposure through scalp and superior palperbral incisions, and the ON crushed for 10 s, 2 mm caudal to the lamina cribrosa with microforceps. Care was taken not to damage the central retinal artery running along the rostral margin of the ON within the dural sheath. In Paper IV, intravitreal PNG implantations were used as regenerative stimuli. One Fisher rat was sacrificed and the sciatic nerve was used as a graft. 1 mm long segments of the nerve were grafted immediately after the crush into the vitreous body through a perforation in the sclera 1 mm dorsal to the optic disc.

3.1.5 Longitudinal studies using MRI

In Paper I, MEMRI was obtained 24 h after intravitreal injection of $MnCl_2$. Additional MR-scans were obtained during 168 h after injection in the time-response experiment. In the longitudinal study of normal and injured ON, rats were re-injected with $MnCl_2$ 20 d after the first injection, and MEMRI obtained 24 h after this (Figure 3.2). In rats with ONC, the first $MnCl_2$-injection was done immediately after the crush.

In Paper II, MRI was obtained at 1 , 12 , 24 and 48 h after intravitreal injection of MnDPDP, 24 h after the $MnCl_2$-injection and 1 , 12 and 24 h after injection of gadodiamide.

In Paper III, MEMRI was obtained 48 h after intravitreal injections of $0 - 3000$ nmol $MnCl_2$. 14 d later, rats were re-injected with 150 nmol $MnCl_2$, and MRI was obtained 48 h after this. In the axonal transport experiment in Paper III, MEMRI was obtained 24 h after injection of 200 nmol $MnCl_2$ directly into the ON.

In Paper IV, MEMRI was obtained 24 h after intravitreal injection of 150 nmol $MnCl_2$. Rats were re-injected with $MnCl_2$ 20 d after the first injection, and MEMRI obtained 24 h after this (figure 3.2). The $MnCl_2$-injection was done immediately after the crush.

Figure 3.2: Longitudinal studies of rats with normal and injured ON (Paper I), and injured ON with intravitreal PNG implantations (Paper IV). $MnCl_2$-injections (Mn), ONC and/or PNG implantations were performed at day 0, and *in vivo* MEMRI obtained 1 d later. Rats were re-injected with $MnCl_2$ at day 20, and *in vivo* MEMRI was obtained 1 d after this, 21 dpl.

3.2 MRI

MRI was performed at 2.35 T or 7 T using Bruker Biospec Avance small animal scanners (Bruker Biospin, Ettlingen, Germany) with 72 mm volume coils for transmission, and actively decoupled quadrature rat head surface coils for receive. Water-cooled BGA-12 gradients were used for all MRI acquisitions. The MR scanner and surface coil are shown in Figure 3.3.

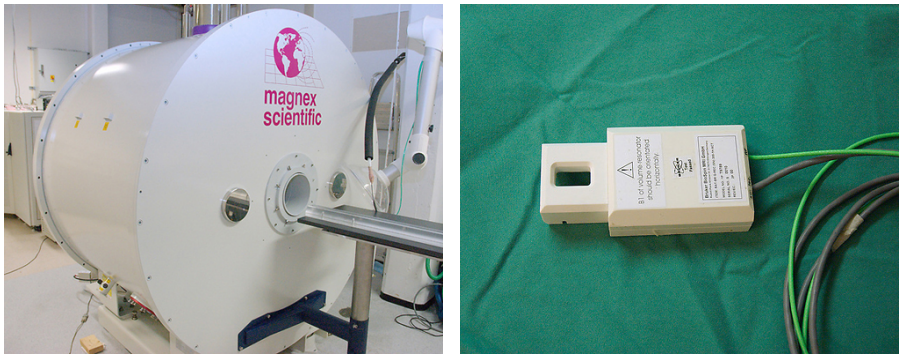

(a) Bruker Biospec 7 T small animal MR scanner.

(b) Quadrature rat head surface coil.

Figure 3.3: MRI was performed with a Bruker Biospec small animal scanner (a) with 72 mm volume coils for transmission, and actively decoupled quadrature rat head surface coils for receive (b).

3.2.1 T_1-weighted MRI

3D data sets of the rat brain were obtained using a T_1-weighted 3D fast low flip angle shot (FLASH) gradient-echo sequence. To correct for the gradually reduced RF signal detected by the surface coil, two additional T_1-weighted 3D FLASH correction scans were performed in coupled and single coil operations, respectively (Papers III and IV only). Details on scan parameters used in the individual papers are listed in table 3.3.

Table 3.3: Scan parameters for the T_1-weighted MEMRI scans used in the experiments. In Papers 1 and 2, equal scan parameters were used. No correction scans were obtained in Papers 1 and 2.

	Paper 1 & 2	Paper 3*	Paper 4
Field strength	2.35 T	7 T	7 T
Magnet	DBX-100	70/20	70/20
Gradients	200 mT/m	400 mT/m	400 mT/m
Heating	circulating air	circulating water	circulating water
Pilot scan	gradient echo	gradient echo	gradient echo
Geometry	10 sag. slices	3 orth slice packages	3 orth slice packages
TR	150 ms	200 ms	200 ms
TE	6 ms	5 ms	5 ms
FOV	5×5 cm^2	6×6 cm^2	5×5 cm^2
Matrix	128 x 128	128 x 128	128 x 128
Acq. time	75 s	25 s	25 s
T1-weighted scan	3D FLASH	3D FLASH	3D FLASH
TR	15 ms	12.5 ms	12.5 ms
TE	4.2 ms	3.7 ms	3.7 ms
Flip angle	25 °C	30 °C	20 °C
FOV	$5 \times 5 \times 2$ cm^3	$4 \times 4 \times 2.5$ cm^3	$4 \times 4 \times 2.3$ cm^3
Matrix	$256 \times 256 \times 128$	$192 \times 192 \times 96$	$192 \times 192 \times 112$
Resolution	$195 \times 195 \times 156$ µm^3	$208 \times 208 \times 260$ µm^3	$208 \times 208 \times 205$ µm^3
NEX	8	8	8
Acq. time	65.5 min	31 min	36 min
Correction scans		3D FLASH	3D FLASH
TR		12.5 ms	12.5 ms
TE		3.7 ms	3.7 ms
Flip angle		30 °C	20 °C
FOV		4 ×4 ×2.5 cm	4 ×4 ×2.3 cm
Matrix		$32 \times 32 \times 16$	$32 \times 32 \times 16$
Resolution		$1250 \times 1250 \times 1562$ µm^3	$1250 \times 1250 \times 1437$ µm^3
NEX		32	24
Acq. time		2.5 min	2.5 min

* The axonal transport experiment in Paper III was done at 2.35 T with equal scan parameters as in Paper I and II.

3.2.2 DTI

In order to obtain reasonable short scan time, DTI-echo planar imaging (EPI) was implemented for the DTI acquisition. EPI is a fast technique that allows rapid DTI imaging.

2D multi-shot (4 segments) DTI-EPI scans with 5 slices containing the ON were obtained with TR = 1500 ms, TE = 32.6 ms, $\Delta = 15$ ms, $\delta = 6$ ms. Diffusion sensitizing gradients along 12 non-collinear directions and 6 b-values in the range of $0 - 3000$ s/mm^2 (5 A0-images, and $300, 600, 1000, 1600, 2300$ and 3000 s/mm^2) were used. The slice thickness was 0.8 mm (no gap), FOV $= 5 \times 5$ cm^2, and acquisition matrix 160×160 (zero filled to 256×256). 4 repetitions were used and the acquisition time was 30 min 48 s. The MEMRI 3D volume was used to locate the appropriate oblique slice package angle for the 2D DTI scans (Figure 3.4).

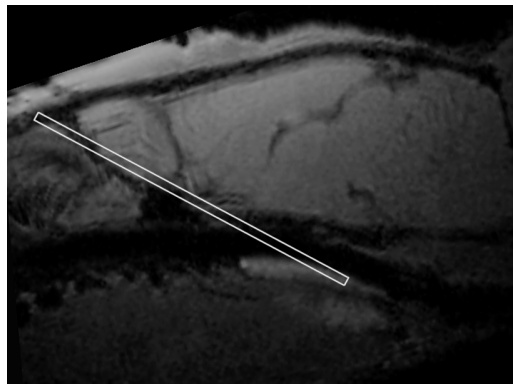

Figure 3.4: The MEMRI 3D volume was used to locate the appropriate oblique slice package angle for the 2D DTI scans in Paper IV. The white box in the mid-sagittal 2D slice of the 3D FLASH image of rat brain indicates the oblique axial imaging plane used for the 2D DTI-EPI acquisition.

3.3 MRI data analysis

3.3.1 Data analysis using ParaVision

In Paper I, the 3D MEMRI datasets were analyzed using software provided by the scanner manufacturer, ParaVision 3.0.1 (Bruker Biospin, Ettlingen, Germany). To quantify Mn^{2+}-enhancement in the control rats 24 h after intravitreal $MnCl_2$-injection, manually drawn regions of interest (ROI) were placed in oblique 2D slices in selected structures (for details, see Paper I) along the Mn^{2+}-enhanced and contralateral non-enhanced visual pathways using the ROI-tool in ParaVision. The ROIs were placed identically in all of the rats and symmetrically in both hemispheres. The mean signal intensities in the ROIs were measured, and the signal-to-noise ratio (SNR) was calculated from [45]

$$SNR = 0.655\frac{S}{SD_{air}} \tag{3.1}$$

where S represents the signal intensity in the ROI of the Mn^{2+}-enhanced area or the contralateral non-enhanced selected area of the visual pathway, and SD_{air} is the mean value of the SD in two ROIs in air.

For the analysis of dose- and time-response of Mn^{2+}-enhancement, the mean signal intensity in ROIs in the Mn^{2+}-enhanced and contralateral non-enhanced visual pathway were measured manually in oblique 2D slices in the 3D volume. The contrast-to-noise ratio (CNR) was calculated from

$$CNR = 0.655\frac{S_{Mn} - S_0}{SD_{air}} \tag{3.2}$$

where S_{Mn} and S_0 represent the signal intensities in the ROI of the chosen structure in the Mn^{2+}-enhanced and contralateral non-enhanced visual pathway.

For the longitudinal studies of rats with normal and injured ON, intensity profiles were calculated from oblique 2D planes showing cross sections of the ON from the retina to the optic foramen (Figure 3.5). The first cross section was placed in the retina, 0.7 mm proximal to the lamina cribrosa. The subsequent cross sections were placed every 0.2 mm from $0-3$ mm, and every 0.4 mm from $3-7$ mm caudally, measured from the lamina cribrosa, for a total of 25 cross sections in each ON. Circular ROIs were placed within the ON in each cross section manually, and the mean signal intensity was measured. The CNR was calculated from the signal intensity at equal distances from the lamina cribrosa in the Mn^{2+}-signal enhanced and non-enhanced ON using the above described formula (3.2).

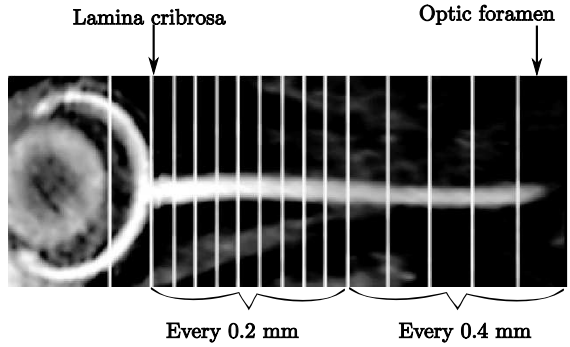

Figure 3.5: In Paper I, the Mn^{2+}-intensity profiles along the ON in the control and ONC groups were assessed by calculating the CNR in cross sections of the ON. The image shows a control rat at 24 h after intravitreal Mn^{2+}-injection. The vertical lines indicate the 2D plane perpendicular to the ON, where the cross sections were drawn using ParaVision 3.0.1, a total of 25 cross sections in each ON. The mean signal intensities in the ROI in each cross section in both the Mn^{2+}-enhanced and non-enhanced ONs were measured and the CNR was computed.

In Paper III, mode of axonal transport was investigated by calculating intensity profiles as described above.

3.3.2 Semiautomatic segmentation procedure

In Paper II, a technique for semiautomatic segmentation of MEMRI data was implemented using Matlab 7.1 (MathWorks, Natick, MA, USA) which included the Image Processing Toolbox. The technique is described in detail in Paper II, and will only be covered briefly here. This segmentation procedure was used to segment the ON in Paper IV.

First, the 3D image was binarized using a global threshold close to the mean signal of the non-enhanced ON. Then morphological segmentation of the Mn^{2+}-enhanced ON was done by a 6-connected region growing from an interactively set seed point within the Mn^{2+}-enhanced ON. The resulting image segment contained the Mn^{2+}-enhanced eye, ON, and part of the brain. In order to separate the ON from the eye and brain, a morphological top-hat transformation was performed, preserving structures not entirely filling the structuring element while translated through the image volume, resulting in a morphological segmented ON. Further-

more, a sliding box segmentation was developed to ensure correct definitions of the coordinates of the ON including start and end points. Two boxes moved along the ON, calculating the center of mass until the density reached either a critical value or 0, indicating that the boxes were apposed to a dense object (e.g. eye or brain), or an "empty" distal end of the ON. The signal in a 1 mm diameter ROI centered on the ON in 2D planes perpendicular to the direction of the ON was measured every 0.2 mm. Due to low SNR, the segmentation procedure failed to segment the non-enhanced nerve. Thus, a regression model based on manually calculated intensity profiles of non-enhanced ON from 10 rats was used to calculate S_0 at all positions along the ON in Paper II. CNR was calculated using the above described formula (3.2).

In Paper IV, the semiautomatic segmentation procedure was used as described above. But because segmentation was performed after surface coil corrections (see 3.3.3), the signal from the non-enhanced ON was uniform throughout the nerve, and the use of a regression model was not necessary.

3.3.3 RF signal correction

In Papers III and IV, the spatially inhomogeneous sensitivity of the coupled-coil was corrected using the set of two low-resolution correction scans with scan parameters as described earlier (see Table 3.3). Using in-house, custom developed software written for Matlab 7.1, the correction scans were interpolated to match the matrix size of the main MRI dataset. Assuming that the sensitivity of the single-coil setup was spatially homogeneous, the MRI signal intensity in a voxel at location (x,y,z) was normalized using the following relation:

$$I_{sc}(x,y,z) = I_{cc}(x,y,z)\frac{C_{sc}(x,y,z)}{C_{cc}(x,y,z)} \tag{3.3}$$

where I_{cc} and C_{sc} is the coupled-coil and single-coil signal intensities in the correction scan datasets, respectively, I_{cc} is the recorded coupled-coil signal intensity in the main MRI dataset, and C_{sc} is the resulting normalized signal intensity.

3.3.4 Normalization of MR data sets

In Paper III, the Statistical Parametric Mapping (SPM5) software package developed for Matlab (Wellcome Department of Imaging, London) was used to normalize all datasets to a chosen template brain. Using a custom developed program written for Matlab 7.1, slices from the normalized 3D volume containing the appropriate regions were chosen and regions of interest (ROI) were drawn

equally in the Mn^{2+}-enhanced and non-enhanced parts of the visual pathway in one data-set and transferred to all other data-sets. CNR was calculated using the above described formula (3.2).

3.3.5 DTI data analysis

The DTI datasets were analysed using custom developed software written in Matlab 7.1. The magnitude operation changes the signal distribution in MR images from Gaussian to Rician, and at low SNR, this introduces a bias that must be taken into account when estimating the apparent diffusion coefficient. A simple least squares fitting of the measured signal to the median value of the probability density function (PDF) was applied. Since averaged magnitude data were used, the PDF could not be expressed in closed form, but had to be calculated numerically as a convolution of Rician distributions (for details, see Kristoffersen 2007 [62]). The noise level, σ, was estimated from a region of interest in the images that were well separated from the object. After estimating σ, the diffusion tensor in each voxel was generated based on 6 different diffusion weightings and 12 different diffusion gradient directions. The tensor's eigenvalues (λ_1, λ_2 and λ_3) were calculated from matrix diagonalization. From the eigenvalues, the DTI-parameters mean diffusivity, FA, $\lambda_{\parallel}$ and $\lambda_{\perp}$ (defined in section 1.5), describing the properties of water diffusion in each voxel, were calculated. Positions were manually selected along the ON in the mean diffusivity-maps starting at the lamina cribrosa. This defined a line which was re-sampled in 0.2 mm resolution and used as co-ordinates of the ON, from which the signal profiles of the ON in the FA-, mean diffusivity-, $\lambda_{\parallel}$- and $\lambda_{\perp}$-maps were calculated by bilinear interpolation.

3.3.6 Statistical analysis

In all experiments, groups were compared using either independent samples, one-samples or paired t-tests in SPSS (SPSS Inc., Chicago, IL, USA), with a significant level of 95%. The statistical analysis is described in detail in the Material and Methods sections of each individual paper.

3.4 Histology

3.4.1 RGC counting using Flurogold

In Papers III and IV, histological counting of the RGC in retina after incrementing doses of intravitreal $MnCl_2$-injections (Paper III) or after ONC with and without PNG and $MnCl_2$-injections (Paper IV) was obtained. The head of the anaesthetised rat was fixed in a stereotactic head holder and the ON was crushed 2 mm from the lamina cribrosa in Paper III, and mid way between the lamina cribrosa and the 0 d ONC lesion site in Paper IV (details on performing the ON crush are given in 3.1.4). 1 µl hydroxystilbamidine (FluroGold (FG), Biotium Inc, Hayward, Ca, USA) was injected into the crush, immediately prior to the intravitreal $MnCl_2$-injection in Paper III, and immediately prior to the second $MnCl_2$-injection at 20 dpl in Paper IV. Rats were killed 48 h after the last $MnCl_2$-injection and the eyes removed, marking the temporal segment with a suture in the sclera. The eye was immersion fixed in 4% paraformaldehyde at 4 °C for 2 h, and the retina whole mounted on a slide, defining the temporal, nasal, superior and inferior retinal quadrants with radial incisions, air dried for 3 h, and mounted in FluorSaveTM reagent (Cabiochem, USA). A 349.0 µm × 440.4 µm counting grid was projected onto the mid radial point of each retinal segment and the total number of FG-filled RGC recorded per grid.

3.4.2 Immunohistochemistry using GAP43

In Paper IV, immunohistochemical staining of the injured ON was obtained 21 dpl. The ON was dissected, straightened on a stiff card and dried in room temperature for a couple of minutes before being immersed in 4% formaldehyde for 2 h at 4 °C. Then the ON was washed in 10 mM PBS, and immersed in 10 % and 20 % sucrose for 2 h each and in 30 % sucrose over night. The ON was removed from the card, embedded in OTC and frozen at −80 °C without disturbing the ON orientation. Using a cryostat (Leica CM3050S, Leica Microsystems, Wetzlar, Germany) with the knife parallel to the long axis of the ON, 5 µm thick frozen sections were cut and mounted onto Superfrost Plus microscope slides, which were dried for 2 h and stored at −20 °C. After drying in 37 °C overnight and 4 d in room temperature, slides were rinsed in Tris-buffered saline (TBS) for 3 × 3 min, and pressure boiled at low pressure in Tris-EDTA pH 9 (TitrplexIII and Tris(hydroxymethyl)-aminomethan) for 12 min, then cooled. Slides were rinsed in TBS for 2 × 3 min and incubated in 2 % BSA in TBS for 10 min. Sections were incubated in monoclonal mouse anti-GAP43 primary antibody (0.5 mg/ml Zymed Laboratories, San Francisco, USA), diluted 1:100,

at 4 °C for $18 - 20$ h in a humidifier chamber. Slides were rinsed in TBS for 2×3 min, and incubated with polyclonal goat anti-mouse FITC secondary antibody (Dako) diluted 1:10 in TBS for 30 min. Finally, slides were rinsed in TBS for 2×3 min and mounted with fluromount medium. Images were obtained using a Nikon Eclipse 90i microscope (Nikon Instruments Europe, Badhoevedorp, The Netherlands) and merged using the photomerge procedure in Adobe Photoshop CS (Adobe Systems Incorporated).

Chapter 4

Summary of papers

Paper I
Manganese-enhanced MRI of the optic visual pathway and optic nerve injury in adult rats.

Marte Thuen, Trond E. Singstad, Tina Bugge Pedersen, Olav Haraldseth, Martin Berry, Axel Sandvig, and Christian Brekken.
Journal of Magnetic Resonance Imaging 22:492–500, 2005.

Mn^{2+} is paramagnetic as well as being a Ca^{2+}-analogue, and is taken up by neurons and transported along axons. The aim of this study was to utilize this in a longitudinal investigation of the normal and injured rat visual pathway, and to define parameters such as dose- and time-response after intravitreal $MnCl_2$-injections.

In the control group 24 h after unilateral intravitreal injection of 150 nmol $MnCl_2$, 3D MEMRI of the rat brain showed Mn^{2+}-enhancement of the visual pathway from the retina to the superior colliculus, with indications of trans-synaptic transport into the cortex. There was a semi-logarithmic relationship between $MnCl_2$-dose and Mn^{2+}-contrast enhancement from $4 - 200$ nmol. Maximum Mn^{2+}-contrast enhancement was seen at 24 h after injection in the ON and at 48 h in the SC, and the Mn^{2+}-contrast decayed gradually to 0 by 168 h. No Mn^{2+}-contrast enhancement was seen distal to the ONC. In the control group, no difference was detected between the first and second 150 nmol $MnCl_2$-injection, 20 d later. In the ONC group, Mn^{2+}-contrast enhancement was reduced proximal to the crush site at 21 dpl compared to 1 dpl, but no difference was detected distal to the lesion between the two time points.

These results demonstrate that MEMRI is a reliable method for longitudinal visualization of the normal visual pathway, and can detect ON injury.

Paper II
Axon tracing in the adult rat optic nerve and tract after intravitreal injection of MnDPDP using a semi-automatic segmentation technique.

Øystein Olsen, Marte Thuen, Martin Berry, Vassili Kovalev, Maria Petrou, Pål Erik Goa, Axel Sandvig, Olav Haraldseth, and Christian Brekken.
Journal of Magnetic Resonance Imaging 27:34–42, 2008.

The aim of this study was to develop and validate an objective technique for 3D segmentation of MEMRI data of the rat ON and optic tract, and to use this technique to investigate the similarities and differences between MnDPDP and $MnCl_2$ as contrast agents for MEMRI of the rat visual pathway, and compare them to the extracellular contrast agent gadodiamide.

Intravitreal injection of MnDPDP resulted in sufficient Mn^{2+}-contrast enhancement of the ON after $12 - 24$ h similar to that after $MnCl_2$-injection. After intravitreal Gd^{3+}-injection, contrast enhancement was seen in the vitreous body only, and not in the retina or ON. The ON was successfully segmented and CNR accurate calculated within 2 minutes.

These results demonstrate that Mn^{2+} was released from MnDPDP in sufficient amounts to obtain functional tracing of the adult rat visual pathway, and that semiautomatic 3D image segmentation and the use of MnDPDP can improve *in vivo* axon tracing in MEMRI. Furthermore, it demonstrates the uniqueness of Mn^{2+} as a intracellular contrast agent, compared to extracellular Gd^{3+}.

Paper III
Manganese-enhanced MRI of the rat visual pathway: acute neural toxicity, contrast enhancement, axon resolution, axonal transport and clearance of Mn^{2+}.

Marte Thuen, Martin Berry, Tina Bugge Pedersen, Pål Erik Goa, Mike Summerfield, Olav Haraldseth, Axel Sandvig, and Christian Brekken.
In press. To be published in Journal of Magnetic Resonance Imaging.

The aim of this study was to provide dose response data for safe and efficient use of $MnCl_2$ as a contrast agent for MEMRI of the rat visual pathway by evaluating RGC toxicity and contrast in MEMRI with increasing dose of $MnCl_2$, MEMRI resolution of axon density, and clearance of Mn^{2+} from the vitreous body after intravitreal injections of $0 - 3000$ nmol $MnCl_2$, and the mode of RGC Mn^{2+}-transport after direct intra-ON injection.

There were no changes in RGC density after intravitreal injections of $MnCl_2 \leq$ 150 nmol and 48 h exposure, and reductions of 12%, 57% and 94% occurred after

300, 1500 and 3000 nmol $MnCl_2$, measured by counting surviving RGC back-filled with Flurogold. CNR in 3D MEMRI of the rat brain increased in the visual pathway with $MnCl_2 \leq 300$ nmol, and decreased when the dose was further increased. Minimum detectable ON axon densities were 125000 axons/mm^2. After injection directly into the ON, CNR > 0 were recorded distally from the injection site, but there was no signal in the retina. After intravitreal injections of doses > 1500 nmol, clearance from the vitreous body was impaired.

These results demonstrate that the optimal dose for MEMRI of the rat visual pathway is $150 - 300$ nmol $MnCl_2$. Higher doses are toxic, causing RGC death, impairment of active clearance from the visual body, and loss of Mn^{2+}-enhancement throughout the visual pathway. Mn^{2+} traffic in RGC axons is mediated mainly by anterograde transport.

Paper IV
Combination of Mn^{2+}-enhanced and diffusion tensor MR imaging gives complementary information about injury and regeneration in the adult rat optic nerve.

Marte Thuen, Øystein Olsen, Martin Berry, Tina Bugge Pedersen, Anders Kristoffersen, Olav Haraldseth, Axel Sandvig, and Christian Brekken.
Accepted for publication in Journal of Magnetic Resonance Imaging.

The main objective of this study was to utilize MEMRI and DTI as tools for detection of ON injury and regeneration in the visual pathway.

ONC reduced RGC survival in retinae by 94 % in rats without intravitreal $MnCl_2$-injections, and by 90 % in rats with $MnCl_2$, compared to non-injured control, measured by counting surviving RGC back-filled with Flurogold. PNG improved RGC survival in retinae. In rats with ONC and PNG, RGC survival in retinae was reduced by 82 % without $MnCl_2$-injection and 74 % with $MnCl_2$-injection. The presence of Mn^{2+} in the non-injured ON did not affect the DTI-derived parameters, and no differences in DTI-derived parameters were detected when comparing the different time-points of the non-injured ON in rats with unilateral ONC. At 1dpl, Mn^{2+}-enhancement was seen in the retina and proximal to the injury site, but no Mn^{2+}-enhancement was detected distally to the injury site. At 21dpl, CNR was increased distally to the injury site compared to that measured at 1dpl. At 1dpl, axonal diffusivity ($\lambda_{\parallel}$) was reduced in the injury site compared to non-injured ON. At 21dpl, $\lambda_{\parallel}$ in the injury site was increased compared to that measured at 1dpl. GAP-43 immunohistochemistry demonstrates axons present in the ON distally to the injury site at 21dpl.

These results demonstrate that MEMRI and DTI are complementary tools for

detecting ON injury, and both techniques are promising for *in vivo* detecting regenerating axons after ON injury.

Chapter 5

Discussion

5.1 Main findings

The main objective of this thesis was to develop and optimize MEMRI and DTI as MRI tools for longitudinal, *in vivo* imaging of the rat visual pathway, and to use these techniques to detect CNS injury and regeneration. In Papers I–III, refinements to the technique of MEMRI were made. The main finding of Paper I was that MEMRI can be used longitudinally to study the normal and injured visual pathway. Intravitreal injection of $MnCl_2$ allows for visualization of the entire visual pathway from the retina to the superior colliculus, in agreement with previous [90, 123]. Furthermore, we have demonstrated that in the mechanically injured adult rat, no Mn^{2+}-enhanced signal was observed in the ON distal to the lesion site, indicating that the injury blocks the active transport of Mn^{2+}. Similar results have been observed in the ON following radiation-induced damage [98], and after mechanically induced injury to the rodent olfactory tract [35] and spinal cord [23, 108]. In Paper II, we demonstrated enhancement of the visual pathway after intravitreal injection of MnDPDP similar to that seen after $MnCl_2$-injections, while no enhancement was seen in the visual pathway after intravitreal injection of gadodiamide. This demonstrated the uniqueness of Mn^{2+}-based contrast agents as intracellular markers for MRI of the CNS. To our knowledge, this is the first study where Mn-DPDP is used as a CNS contrast agent, previous animal studies using Mn-DPDP have mainly focused on heart or liver MR imaging [44, 61, 74]. The toxicity of Mn^{2+} is well documented, but few studies have addressed acute toxic reactions after local injections into the CNS. In Paper III, we show that the optimal $MnCl_2$-dose for MEMRI of the rat visual pathway after intravitreal injections was in the range of $150 - 300$ nmol, providing sufficient tissue contrast without being toxic. High doses of $MnCl_2$ (500 nmol and higher) were toxic, leading to massive RGC death. Furthermore, we have demonstrated that there was a strong correlation between the number of axons and CNR in MEMRI, and that viable axons were necessary for Mn^{2+}-transport.

Regeneration in the CNS after injury and therapeutic intervention have been studied extensively using histological tract tracing methods, however, *in vivo* methods for detecting regeneration after injury are wanted. Three main findings of this thesis demonstrate the potential for MEMRI as a possible tool for investigating regeneration after axonal injury:

- MEMRI can be performed longitudinally.
- The transport of Mn^{2+} is blocked after ON injury.
- Viable axons are needed for transport of Mn^{2+}.

In Paper IV, we demonstrate using MEMRI increased Mn^{2+}-enhancement in the distal ON after injury and intravitreal PNG, indicating that axons have regenerated through the injury and beyond. To our knowledge, no previous studies have investigated regeneration in the ON after injury and treatment using MEMRI. However, after an 80% spinal cord transection in mice, antibody therapy promoted axonal survival of spared axons and possibly induced regeneration after injury. This was demonstrated by increased Mn^{2+}-enhancement in the spinal cord distal to the injury site [108], supporting our findings in the rat ON. As a complementary method to MEMRI, DTI was defined as a tool for visualization of the ON in Paper IV. Most previous studies of the ON using DTI have used spin echo (SE)-DTI, which is less prone to image distortions, but also requires long scan time, making *in vivo* scanning in combination with other MR protocols difficult. In this thesis, we combine *in vivo* DTI with MEMRI by using the rapid imaging technique DTI-EPI. We found that $\lambda_{\parallel}$ was reduced in the injury site, which is in agreement with previous findings [105, 109, 110, 129]. To our knowledge, no previous studies have investigated regeneration in the ON after injury and treatment using DTI. The main findings of Paper IV were that MEMRI and DTI give complementary information about functional and structural changes in CNS, and both methods detect axonal injury in the ON, and give indications of axonal regeneration after injury and intravitreal PNG.

5.2 Methodological considerations

5.2.1 MEMRI

In MR imaging, the goal is to quickly obtain high quality data with high SNR, high CNR and good image resolution. When scanning live objects, time is often the limiting factor. In every protocol, parameters such as TR, TE, flip angle, field of view (FOV), slice thickness, matrix size, number of averages (NEX) and

receiver bandwidth must be optimized to obtain the best image quality possible within the time frame available. The choices of TR, TE and flip angle determine if the image will be proton density, T_1- or T_2-weighted, and influence the image contrast. Increasing TR will increase SNR, but also the acquisition time. Choosing a large matrix size and thin slices will give a high resolution image, however, this will also increase the scan time and reduce SNR. Scan time increases linearly with the number of averages (NEX), while SNR increases as $\sqrt{\text{NEX}}$, due to the presence of random noise in the data. Reducing the receiver bandwidth will reduce the noise, which will increase SNR. However, this will also increase the minimum TE and increase chemical shift artifacts. The field strength and type of coil also greatly affect SNR [51, 127].

All MEMRI acquisitions in this thesis were obtained using a T_1-weighted 3D FLASH protocol. T_1-weighting is obtained by acquiring an MR-scan with low TR and low TE. In a 3D volume acquisition, the entire set of continuous slices is excited for each TR, resulting in a 3D k-space matrix of raw data that is reconstructed by 3D Fourier transform. 3D acquisitions will usually increase the scan time compared to 2D, but SNR will increase, and the slice thickness can be drastically reduced, allowing reduced partial volume effects and better image resolution [18]. The 3D FLASH sequence used in Papers I and II was based on the protocol used by Watanabe et al [123], where 3D MEMRI of the visual pathway was obtained at 2.35 T with a similar magnet as our system. This protocol was optimized with regards to flip angle, to obtain high SNR within a reasonable scan time. Before data collection for Paper I, the protocol was tested at our system, and it was found that no further optimalization was necessary.

The MRI-acquisitions in Papers I and II were performed at 2.35 T, while in Papers III and IV, MRI was performed at 7 T. Theoretically, SNR should increase linearly with increasing field strength [43]. However, susceptibility and chemical shift artifacts increase with higher fields, as well as a lengthening of T_1 and a shortening of T_2 [75]. Thus, the observed increase in SNR is usually not as high as theoretically expected [21]. The increase in SNR can for example be used to reduce the scan time (by reducing TR or NEX), or increase the resolution. The latter is illustrated in Figure 5.1, where the increased SNR at 7 T is used to increase the resolution in a frog brain within equal acquisition times. Going from 2.35 T to 7 T (Paper I and II versus Paper III), TR in the MEMRI rat brain protocol was reduced from 15 ms to 12.5 ms (Table 3.3). This, in addition to small decrease in resolution, lead to a scan time of approximately 30 min, compared to 1 h in Papers I and II. Still, an increase in SNR of approximately 50% was obtained. The flip angle was found not to affect SNR or CNR very much within the range of 20 to 30°.

A surface coil was used for all MR imaging. This greatly increases SNR, however,

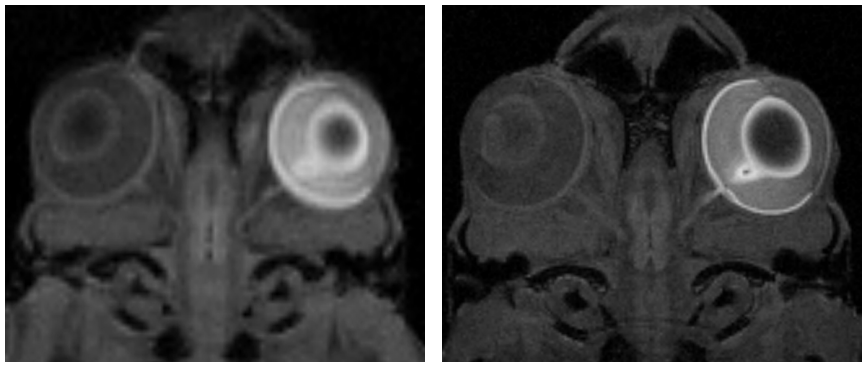

(a) Field strength: 2.35 T,
Resolution: $273 \times 234 \times 313$ μm^3,
Number of averages: 16,
Acquisition time: 32 min.

(b) Field strength: 7 T,
Resolution: $136 \times 136 \times 156$ μm^3,
Number of averages: 4,
Acquisition time: 32 min.

Figure 5.1: Oblique 2D slices from 3D MEMRI of the frog brain 48 h after intravitreal 150 nmol $MnCl_2$-injection showing the retina and ON at 2.35 T (a) and 7 T (b). The same frog is imaged at both field strength. Both scans were performed with the same acquisition time, and the increased SNR at 7 T was used to increase the resolution and reduce NEX. All other scan parameters were the same, and a quadrature rat head surface coil was used in both acquisitions.

the RF signal detected is gradually reduced as the distance form the coil to the tissue increases. In the rat visual pathway, the ON projects ventrally from the retina, away from the dorsally located surface coil, resulting in an expected gradually reduced signal along the ON. To adjust for this, the CNR was calculated from the signal intensity in the Mn^{2+}-enhanced and contralateral non-enhanced ON, at positions along the ON located equidistant from the surface coil. However, because of the increased signal in the $MnCl_2$-injected ON compared to the non-injected ON, this still causes a reduction in the CNR with increasing distance between the ON and the surface coil in Paper I and II (Paper I; Figure 7 and Paper II; Figure 8). In Paper III and IV, low resolution correction scans with equal parameters as the high resolution 3D FLASH sequence was obtained in single and coupled operation settings, to correct for the gradually reduced detection area of the surface coil (see Table 3.3). This corrected for almost all of the gradually reduced signal (Figure 5.2), thus, the observed fall in CNR is mostly caused by the use of a surface coil. However, the fall in CNR could also be

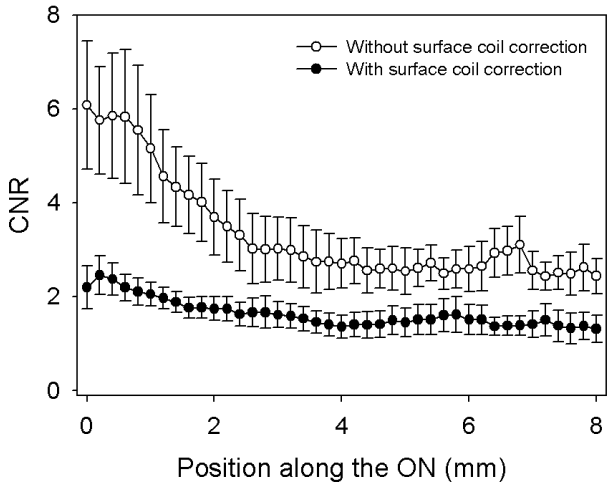

Figure 5.2: CNR ± SEM profiles along the ON after intravitreal injections of 150 nmol $MnCl_2$ in 8 normal rats without surface coil correction (open circles) and with surface coil correction (filled circles).

attributed to temporospatial effects caused by axonal transport mechanisms of Mn^{2+}. The uptake of Mn^{2+} by RGC, the potential combination of active transport and passive diffusion, and the possible clearance of Mn^{2+} from the ON are all factors that may have contributed to the characteristic CNR profiles observed

in rats with normal ON.

In Paper I, the ROI tool in ParaVision was used to analyze the data. The procedure was very time consuming, and required high degree of user interaction which was subjected to possible user bias. Furthermore, the reconstructed 2D slices perpendicular to the ON were limited to 8-bit resolution, not utilizing the whole 16-bit range of the original 3D data set. This could reduce the sensitivity and possible not detect differences in CNR that were detectable in the 16-bit data volume. Thus, the was a need for a more automated and efficient segmentation procedure, which was developed in Paper II. Here, the ON was automatically segmented based on a manually set seed point within the ON, a highly unbiased and efficient procedure using the whole 16-bit range. The procedure of Paper II needed a minimal CNR in the ON. Thus, it could not be used in Paper III, where CNR was close to zero in the visual pathway after high doses of $MnCl_2$. Furthermore, the segmentation procedure segmented the ON and optic tract only, not the SC, which was examined in Paper III. To reduce user bias and increase efficiency compared to the procedure used in Paper I, all MEMRI data sets in Paper III were normalized to a chosen template brain. ROIs were drawn manually in one dataset and transferred to all the other data-sets. In Paper IV, the semi-automatic segmentation procedure developed in Paper II was used for data analysis.

The experiments of this thesis have all been using T_1-weighted imaging. T_1-*mapping* is more sensitive to changes in T_1 that T_1-weighing, and would provide the true T_1-value of each voxel in the data volume. T_1-mapping of the entire rat brain is possible using for example the Look–Locker method in either multiple 2D slices or a 3D volume [34, 52], however, the technique is challenging compared to the 3D weighted FLASH sequence with regards to obtaining good image quality and post processing procedures.

5.2.2 DTI

DTI of the animal brain is challenging due to the small nerve fiber bundles compared to humans. SE-DTI has produced good image quality DTI maps of rodents; however, the scan time is long, up to several hours [109], making it difficult to combine *in vivo* DTI with other protocols. EPI is a very fast imaging technique that allows rapid *in vivo* DTI of the animal brain. However, EPI is prone to eddy current- and chemical shift artifacts, and image distortions due to field inhomogeneity and magnetic susceptibility variations [18]. DTI-EPI of the ON is particular challenging because of its small size, uncontrolled motion, air in the nasal cavity causing susceptibility effects, and high signal from fat and

cerebrospinal fluid surrounding the ON [128]. In spite of these difficulties, we have developed a DTI-EPI protocol which produced good quality images of the ON *in vivo* with few geometrical distortions. Furthermore, by comparing DTI results form control ON with or without Mn^{2+}-enhancement, we were able to rule out interference from Mn^{2+} with regards to the DTI-derived measures. The parameters that mostly affected the image quality was increasing the receiver bandwidth to 500000 Hz, and introducing multi shot EPI (number of shots = 4), both of which were crucial for obtaining satisfactory image quality at our system. Increasing the receiver bandwidth reduces SNR, but will also reduce chemical shift artifacts. Multi shot EPI can yield better image quality because of better SNR, reduced blurring, less distortions and lower ghost intensity [18]. However, the scan time is increased and multi shot EPI is more sensitive to motion. Although pilot studies revealed better image quality *ex vivo*, satisfactory image quality was accomplished *in vivo*, and no gating was necessary. Better MR hardware, especially improved shim strength, would increase field homogeneity, and could improve the EPI protocol.

5.2.3 MEMRI and DTI

MEMRI and DTI are complementary methods with sensitivity for *in vivo* tracing of normal, injured and regenerating axons in the ON. Good image quality was easily obtained using the FLASH-sequence for T_1-weighted MEMRI, while DTI-EPI was prone to susceptibility-related artifacts, and geometrical distortions compared to MEMRI. Thus, DTI is a more challenging imaging technique than MEMRI with regards to protocol optimalization. However, DTI-EPI has the advantage of being completely non-invasive with no need for contrast agent injections. Further pulse sequence optimalization of both MEMRI and DTI protocols, as well as more sophisticated post-processing methods and better MR hardware can possible improve both sensitivity and image quality. In particular, 3D T_1-mapping has recently been shown to improve Mn^{2+}-sensitivity in rodent neural tract tracing by MEMRI [34]. Furthermore, inversion recovery preparations might improve T_1-weighted contrast, especially important when applying this technique to even higher magnetic fields strengths due to the inherent convergence of T_1 relaxation times.

5.3 Mn^{2+} as a contrast agent

5.3.1 Mn^{2+} and toxicity

The toxicity of Mn^{2+} in the nervous system is well documented [7, 36, 97]. In humans, long term exposure to Mn^{2+} induces parkinsonian symptoms, including headaches, memory loss, emotional instability, rigidity, tremors, seizures and death [7, 36], and animal studies have shown neuronal degeneration after $MnCl_2$ injections into the striatum [26]. However, little is known about the acute effects of $MnCl_2$ when used as a contrast agent for MEMRI. Bearer et al. [13] recently reported a transient disruption of retinal electrical activity after 100 nmol (0.5 µl 200 mM) intravitreal injection of $MnCl_2$ in mice, as well as 25% loss of RGC after 4 months. In MEMRI, high Mn^{2+}-enhanced tissue contrast, but without introducing toxic effects is wanted. In Paper I, we showed that increasing the dose of $MnCl_2$ from 0 to 200 nmol lead to a gradually increase in CNR in the ON. In Paper III, a wider range of $MnCl_2$-doses from $0 - 3000$ nmol was investigated. Here, we observed a gradually increase in CNR in the ON and SC as the dose was increased from $0 - 300$ nmol, and a decrease in CNR when the dose was increased from $300 - 3000$ nmol. The decrease in CNR with high doses of $MnCl_2$ was attributed to breakdown of axonal transport mechanisms and RGC degeneration caused by Mn^{2+}-toxicity. Based on these results, the optimal dose for MEMRI of the visual pathway is in the range of $150 - 300$ nmol. This will give maximal CNR without introducing severe RGC toxicity. In Paper I, rats were given serial intravitreal $MnCl_2$-injections of 150 nmol at 0 d and 20 d, and MEMRI at 1 d and 21 d showed no difference in CNR between the two time-points, demonstrating that longitudinal MEMRI is feasible. However, long term toxic effects caused by $MnCl_2$ was not investigated in detail in this thesis.

Several strategies can be used to reduce the Mn^{2+}-dose. T_1-mapping is a quantitative imaging technique providing the T_1-value in each voxel of the data volume, and is more sensitive to changes in Mn^{2+}-enhancement that T_1-weighted imaging. Thus, the Mn^{2+}-dose needed for sufficient tissue contrast can be reduced. To reduce the high initial concentrations after local injections of $MnCl_2$ into the CNS, Mn^{2+}-releasing contrast agents such as MnDPDP (Paper II) or alginate capsules can be used. However, attention must also be given to safe ways of administrating Mn^{2+} into the specific brain regions, and clearance versus accumulation of Mn^{2+} in the brain.

5.3.2 Can Mn^{2+} have a therapeutic effect?

In Paper IV, toxic effects of two serial doses of 150 nmol $MnCl_2$ on RGC survival in retina in rats with ONC was investigated. We feared that injured axons could be more sensitive to toxic reactions of an assumed non-toxic dose of Mn^{2+} than non-injured axons. Surprisingly, the current results suggest that $MnCl_2$ had a protective effect on RGC survival after ONC. There are several explanations for our observations. Apoptosis after ONC is triggered by the entry of Ca^{2+} into RGC [99], and since Mn^{2+} enter RGC through voltage gated Ca^{2+}-channels, non-toxic concentrations of Mn^{2+} may competitively block Ca^{2+} entry thereby protect against apoptosis. Furthermore, ONC may cause the release of free radicals which cause oxidative stress and cellular damage [49]. Mn^{2+} has the ability to act as a scavenger, protecting RGC against oxidative stress [5, 10, 27]. Similar observations of Mn^{2+}-protection have been observed when the Mn^{2+}-containing and Mn^{2+}-releasing contrast agent MnDPDP (Teslascan™) has been introduced after acute liver injury and in hearts subjected to cardiac infarction. Furthermore, it has been shown that MnDPDP has the potential to enhance anticancer drug treatment by protecting normal cells as well as increasing the activity of the anticancer agent [16, 27]. Further research is needed to fully understand these possible therapeutic effects of Mn^{2+}.

5.3.3 Uptake, binding, transport and clearance of Mn^{2+}

After injection, there is an uptake of Mn^{2+}, and a subsequent transport of Mn^{2+} along the axons. Little is known about the dynamics of uptake versus transport, for example if the transport rate is limited by the uptake of Mn^{2+}, or the subsequent transport mechanisms, or both. Mn^{2+} is taken up by voltage gated Ca^{2+}-channels [82], which are present in great numbers in dendrites of the cell body. Mn^{2+} can also enter through other Ca^{2+}-transporters such as the Ca^{2+}-pump mediated by ATP and the Na^{+}/Ca^{2+}-exchanger [91]. A reduced uptake of Mn^{2+} has been observed after administration of the Ca^{2+}-channel blocker diltiazem [88].

The effect of a substance on proton relaxation rate is known as relaxivity [65]. Water molecules tumbles much faster than the Larmor frequency, resulting in inefficient relaxation, which is demonstrated by long T_1 and T_2 relaxation times. Paramagnetic substances, such as Mn^{2+}, are strong magnetic dipoles that when placed in the presence of tumbling water protons, creates fluctuation in the magnetic field because of dipole-dipole interactions between electrons and protons. This will reduce the T_1 relaxation times of the nearby protons, and result in increased signal in T_1-weighted images [127]. Bound Mn^{2+} have a stronger re-

laxivity (i.e. stronger T_1-effect) compared to free Mn^{2+} [58]. This can be explained by binding of Mn^{2+}-ions to macromolecules, which will greatly reduce the molecular tumbling rate of the paramagnetic center, leading to a more efficient dipolar interaction with surrounding protons. Intracellularly, Mn^{2+}-ions can bind to a variety of macromolecules, and be transported into organelles such as mitochondria and endoplasmatic reticulum, or move freely in the cytosol. The strong T_1-effect observed in these experiments suggests that most Mn^{2+}-ions are bound to macromolecules within the RGC. The exact locations of the Mn^{2+}-ions within the cell, remain unknown.

Several observations indicate that there is an active transport of Mn^{2+} inside axons. In Paper I, we show that no Mn^{2+}-enhancement was detected distal to the ON injury, demonstrating that mechanically injuring the axons blocks the transport of Mn^{2+}. Furthermore, in Paper III, no Mn^{2+}-enhancement was observed in the visual pathway after high doses of $MnCl_2$ indicating that viable axons are needed for transport of Mn^{2+}. These results are supported by previous findings; Paulter and Koretsky demonstrated that the transport of Mn^{2+} is blocked after administration of the microtubule disrupting agent colchicine [88]. Passive diffusion could also contribute to the transport of Mn^{2+}. Passive diffusion of Mn^{2+} has been observed after direct injection into the striatum and amygdala [89]. Separation of the two transport mechanisms is often difficult. After ONC, no Mn^{2+}-was seen distal to the crush site (Paper I). If passive the diffusion was the main mechanism of Mn^{2+}-transport, Mn^{2+}-enhancement distal to the crush site would be expected. However, Mn^{2+}-diffusion could be blocked by the ONC scar tissue, or Mn^{2+} could be removed from the ON by blood in the crush, and thus not be observed in the distal ON, even if it was transported passively within the ON. It has been suggested that Mn^{2+} mainly is transported anterogradely [104], but retrograde transport of Mn^{2+} has been recorded in the mouse striatum and amygdala [89]. After intra-ON injection, we observe Mn^{2+}-enhancement distal to the injection site (Paper III). Proximal, some Mn^{2+}-enhancement is observed close to the injection site, but not in the retina. This indicates that a small component of the transport might be mediated by passive diffusion at a speed not high enough to reach the retina within 24 h. Furthermore, this indicates that anterograde, not retrograde transport is the main direction of Mn^{2+}-traffic within the ON.

After intravitreal injection, the maximal CNR was seen in ON after 24 h and in the SC after 48 h, demonstrating the temporospatial movement of Mn^{2+} through the visual pathway. The distance between the ON and SC is approximately 22 mm. Using this, we can estimate the rate of Mn^{2+}-transport to be approximately 1 mm/h. This is lower that the rates of $2-5$ mm/h recorded in the ON by Pautler et al and Bearer et al [13, 90]. Our estimate was, however, not based

on a dedicated transport rate experiment, but derived from an experiment where the main purpose was to investigate clearance of Mn^{2+} from the visual pathway. Because a variety of molecules/organelles might be involved in the transport of Mn^{2+}, the Mn^{2+}-transport might consist of several components, with different transport rates. A dedicated transport rate experiment could tell us more about which structures within the axons that are involved in the transport of Mn^{2+}, and the transport rates of Mn^{2+}-traffic. Furthermore, blocking/impairment of various structures within the axons could provide information about which components of the axons that are involved in the transport of Mn^{2+}.

Mn^{2+} can traverse the synaptic cleft and be taken up in the post-synaptic membrane [111]. Using MEMRI, trans-synaptic transport of Mn^{2+} has been observed in the olfactory pathway, striatum and amygdala [89, 90, 100]. In the visual pathway, RGC axons project from the retina to the LGN and SC without synapses, however, in the LGN, visual information is transferred via synaptic connections through the optic radiation to layer IV in the primary visual cortex. In our experiments, we did not observe significant Mn^{2+}-enhancement of the primary visual cortex. As the amount of Mn^{2+} is reduced when crossing the synapse, MEMRI sensitivity could limit the detection of Mn^{2+} in the post-synaptic areas. Nevertheless, Lindsey et al recently demonstrated Mn^{2+}-enhancement in the mouse visual cortex after intravitreal injection. Although detection of trans-synaptic Mn^{2+}-transport has not been the main focus of this PhD-thesis, we have detected Mn^{2+}-enhancement in a subcortical area outside the visual pathway, most likely the CA3 region of the hippocampus, also observed by others [122]. This suggests that Mn^{2+} is released, either through the synapses in the LGN, and/or unspecifically throughout the visual pathway into for example the ventricles, and a subsequent uptake of Mn^{2+} into the hippocampal area. Accumulation of Mn^{2+} in the hippocampal formation has also been observed after systemic injection [122], suggesting high affinity for Mn^{2+} in the hippocampal region.

In Paper I, we show that Mn^{2+} is cleared from the visual pathway 168 h after intravitreal injection of 150 nmol $MnCl_2$. The exact mechanisms for clearance of Mn^{2+} from the visual pathway are not known, but systemic venous and lymph vessels are believed to be involved. Mn^{2+} is cleared from the body by biliary, pancreatic and urinary excretion [7], however, it has been shown that some Mn^{2+} can accumulate in the brain [7, 48]. Even if Mn^{2+} is cleared from the visual pathway by one week, the clearance rates from the brain and rest of the body have not been investigated here.

5.3.4 Mn^{2+} and other contrast agents

Gadolinium (Gd^{3+})-based contrast agents are by far the most common contrast agents used in clinically MRI. Similarly to Mn^{2+}, Gd^{3+} is a paramagnetic heavy metal that reduces T_1. In Gd^{3+}-based contrast agents, Gd^{3+} is chelated into a stable complex and is not released from this complex within the body. The complex is usually administrated intravenously, and released from the capillaries into interstitial space [17]. As the uptake and clearance of Gd^{3+}-complexes from normal and abnormal tissue differers, MRI can separate pathological tissue such as tumors and stroke from healthy tissue. However, in contrast to Mn^{2+}, the Gd^{3+}-complex is not taken up into cells, and thus is an *un*specific contrast agent. As demonstrated in Paper II, Gd^{3+} is not taken up into the retina or ON after intravitreous injection, but is present in the vitreous for a period of at least 12 h, and is cleared gradually within 24 h, most likely by superficial retinal veins. This demonstrates the uniqueness of Mn^{2+} as a MRI contrast agent.

5.4 CNS injury and regeneration

Before MEMRI can be considered as a tool for detection of axonal regeneration, some conditions need to be fulfilled. Three of the major findings of this thesis address these conditions. Firstly, MEMRI can be used as a longitudinal tool. After clearance of Mn^{2+} from the visual pathway (by $\sim$7 d), rats can be re-injected with $MnCl_2$, allowing for longitudinal monitoring of animals after injury. Secondly, the transport of Mn^{2+} is blocked after ON injury, enabling detection of the injury. Thirdly, viable axons are necessary for Mn^{2+}-transport, making it possible to detect regenerating axons. Thus, Mn^{2+} is transported actively in axons, and MEMRI is a measure of axonal function. Without these conditions fulfilled, the use MEMRI as a tool for detection of regeneration in the CNS would be difficult.

These findings demonstrate that MEMRI *as a method*, has the potential of detecting regenerating axons. However, several obstacles exists. Regeneration after intravitreal PNG is well documented using traditional histological tract tracing methods [20, 38, 47]. But the amount of CNS axons that regenerate after injury and stimulation is limited to maximum 10%, and the sensitivity of MEMRI is low compared to histological tract tracing methods. Thus, even if these regenerating axons have the ability to transport Mn^{2+}, it might not be enough axons with Mn^{2+} present to reach a level detectable by MEMRI. Furthermore, the resolution of MEMRI is low compared to histology. While histological methods can separate individual axons, this is far from possible using MEMRI. However, MEMRI

has the major advantage of being a longitudinal tool for *in vivo* investigation. Future advances in developing regenerating stimuli would increase the amount of expected regeneration, making MEMRI an even more attractive tool. Additionally, future improvements in MR technology can increase both sensitivity and resolution. While MEMRI hardly will be as good as histological methods, the gap between the methods will decrease.

No Mn^{2+}-enhanced signal was detected distal to the injury site 1 dpl. Proximal to the injury site, Mn^{2+}-signal enhancement was increased compared to non-injured control ON with intravitreal $MnCl_2$ (Paper I; Figure 7). This can be attributed to accumulation of Mn^{2+} in the proximal ON caused by disruption in downstream axonal transport in the injury site. CNR in MEMRI was increased at the lesion site and distally at 21 dpl compared to 1 dpl in rat with ON injury and intravitreal PNG implantations (Paper IV), while no difference was seen in rats with ON injury only (Paper I). This indicates that axons have regenerated through the injury site and beyond after injury and PNG implantation. These results were confirmed by GAP-43 immunohistochemistry, that showed the presence of axons in the ON distal to the injury site. However, no ultra structural methods that can pinpoint the exact location of the Mn^{2+}-ions within the axons are easily available. Thus, our results give only an indication of regeneration that has to be confirmed by future studies.

$\lambda_{\parallel}$ derived from DTI-measurements has been suggested as a biomarker for axonal damage [105, 6, 115], and is the strongest candidate of the DTI-parameters (FA, mean diffusivity, $\lambda_{\parallel}$ and $\lambda_{\perp}$) to describe axonal regeneration. $\lambda_{\parallel}$ was reduced in the injury site at 1 dpl, demonstrating that DTI can detect axonal injury. Previous DTI-studies of axonal injury without regenerative stimulation have shown no difference, or an additional decrease in $\lambda_{\parallel}$ in the chronic phase after injury compared to the acute phase [109, 110, 129]. Here, we demonstrate an increase in $\lambda_{\parallel}$ in the injury site at 21dpl compared to that measured at 1dpl. This suggests a normalization of axonal structures within the ON in the chronic phase, approaching values of $\lambda_{\parallel}$ for the non-injured ON, and indicates that axonal regeneration can be detected using DTI.

Taken together, results from this thesis, which are confirmed by GAP-43 immunohistochemistry, indicate that MEMRI and DTI can detect regeneration after injury and intravitreal PNG in the rat visual pathway.

5.5 Clinical considerations

In this thesis, MEMRI and DTI are defined as tools for studying the normal, injured and regenerating visual pathway. Parameters such as dose- and time-response of Mn^{2+}-enhancement, toxicity of Mn^{2+} and mode of Mn^{2+}-transport were specified for MEMRI, and a DTI-EPI protocol for *in vivo* acquisitions was optimized. This constitutes refinements to the techniques of MEMRI and DTI, and can be applied to a variety of methods in experimental animal research. Thus, MEMRI and DTI are valuable techniques in animal research, and can be used for example in development and testing of new therapeutics for regeneration after CNS injury and other neurodegenerative diseases. When a promising therapeutic is developed, this can be transferred into clinical trials, and ultimately, if successful, becoming part of routine clinical treatment. MEMRI and DTI can also be used in other aspects of preclinical CNS research, to learn more about for example epilepsy, glaucoma and stroke [1, 32, 72, 120] before this knowledge is transferred into patient care.

However, direct clinical applications of DTI and MEMRI exist. DTI is currently being introduced as a clinical tool to map white matter tracts of the human brain. DTI is non-invasive and without the need for contrast agents, and because of larger nerve bundle size, DTI of the human brain can be obtained more easily that of the animal brain. However, to define and refine DTI as a tool for detection of CNS injury and regeneration, the controlled settings of animal research is needed. Introducing MEMRI of the CNS into the clinic is not equally straight forward. The major obstacle is the toxicity of Mn^{2+}. However, the high initial concentrations of Mn^{2+} could potentially be reduced by developing new slow-release Mn^{2+}-contrast agents. Furthermore, the constant improvement in RF coil technology and MR pulse sequences could improve MEMRI sensitivity, so that the Mn^{2+}-dose needed for sufficient tissue contrast can be reduced. This could potentially facilitate future transition into clinical CNS applications. Given that the limitations of MEMRI could be overcome, several potential future clinical applications of MEMRI exist. With increasing MR field strengths, T_1 increases, and separation of grey/white matter contrast becomes more difficult. Mn^{2+} could increase white matter contrast at higher fields and facilitate anatomical imaging of the human brain. Furthermore, MEMRI has the potential to detect structural and functional changes in the CNS, and be a complementary technique to applications such as DTI and BOLD fMRI, in the latter case because Mn^{2+} accumulates in activated areas of the brain, enabling mapping of brain activation. This is of potential interest in epilepsy and brain tumor surgery. MEMRI could also become a powerful tool for cellular imaging of neurodegenerative diseases and monitoring response to regenerative therapy also in humans. Examples of

the latter are differentiation of implanted stem cells and regeneration of axonal connections after spinal cord injury. It must be emphasized that more work is needed to reveal the full potential of clinical MEMRI of the CNS.

5.6 Future perspectives

This thesis has provided refinements to MEMRI, however, much is still unknown about the transport mechanisms of Mn^{2+} in axons. Future studies could tell us more about the rate and direction of Mn^{2+}-traffic within the axons, and which subcellular compartments within the axons are involved in transporting Mn^{2+}. Also, there is a need for an easily available method for ultrastructural detection of Mn^{2+}, to pinpoint the exact location of Mn^{2+} within the cell. Future protocol optimalization and development of new MR hardware and post processing tools will improve MEMRI and DTI sensitivity and specificity. Thus, MEMRI and DTI have the potential for becoming important tools for monitoring CNS injury and regeneration, both in animal models, and in patient care.

5.7 Conclusion

Methods for *in vivo* longitudinal MR imaging using MEMRI and DTI have been established, with the purpose of studying the normal, injured and regenerating visual pathway. Both MEMRI and DTI can visualize the normal ON, detect ON injury and are promising tools for detecting regeneration after ON injury. MEMRI detects the axons ability to transport Mn^{2+}, and thus is a measure of axonal function. DTI is a measure of water diffusion, reflecting mainly structural changes in the ON. Thus, MEMRI and DTI are truly complementary methods for detecting axonal injury and regeneration.

Bibliography

[1] S. Alvestad, P.E. Goa, H. Qu, Ø. Risa, C. Brekken, U. Sonnewald, O. Haraldseth, J. Hammer, O.P. Ottersen, and A. Håberg. In vivo mapping of temporospatial changes in manganese enhancement in rat brain during epileptogenesis. *Neuroimage*, 38:57–66, 2007.

[2] I. Aoki, T. Ebisu, C. Tanaka, K. Katsuta, A. Fujikawa, M. Umeda, T. Takegami, E. M. Shapiro, and S. Naruse. Detection of the anoxic depolarization of focal ischemia using manganese-enhanced MRI. *Magn. Reson. Med.*, 50:7–12, 2003.

[3] I. Aoki, C. Tanaka, T. Takegami, T. Ebisu, M. Umeda, M. Fukunaga, K. Fukuda, A.C. Silva, and A.P. Koretsky. Dynamic activity-induced manganese-dependent contrast magnetic resonance imaging (DAIM MRI). *Magn. Reson. Med.*, 48:927–933, 2002.

[4] I. Aoki, Y.J. Wu, A.C. Silva, R.M. Lynch, and A.P. Koretsky. In vivo detection of neuroarchitecture in the rodent brain using manganese-enhanced MRI. *Neuroimage*, 22:1046–1059, 2004.

[5] F.S. Archibald and I. Fridovich. The scavenging of superoxide radical by manganese complexes: In vitro. *Arch. Biochem. Biophys.*, 214:452–463, 1982.

[6] K. Arfanakis, V.M. Haughton, J.D. Carew, B.P. Rogers, R. J. Dempsey, and M.E. Meyerand. Diffusion tensor MR imaging in diffuse axonal injury. *AJNR Am. J. Neuroradiol*, 23:794–802, 2003.

[7] M. Aschner, K.M. Erikson, and D.C. Dorman. Manganese dosimetry: Species differences and implications for neurotoxicity. *Crit. Rev. Toxicol.*, 35:1–32, 2005.

[8] M. Aschner and M. Gannon. Manganese (Mn) transport across the rat blood-brain barrier: Saturable and transferrin-dependent transport mechanisms. *Brain Res. Bull.*, 33:345–349, 2004.

[9] M. Aschner, T.R. Guilarte, J.S. Schneider, and W. Zheng. Manganese: Recent advances in understanding its transport and neurotoxicity. *Toxicol Appl Pharmacol*, 221:131–147, 2007.

[10] A. Asplund, D. Grant, and J.O.G. Karlsson. Mangafodipir (MnDPDP)- and $MnCl_2$-induced endothelium-dependent relaxation in bovine mesenteric arteries. *J. Pharmacol. Exp. Ther.*, 271:609–614, 1994.

[11] M. Bader, M.C. Dietz, A. Ihrig, and G. Triebig. Biomonitoring of manganese in blood, urine and axillary hair following low-dose exposure during the manufacture of dry cell batteries. *Int. Arch. Occup. Environ. Health*, 72:644–649, 1999.

[12] P.J. Basser, J. Mattiello, and D. LeBihan. MR diffusion *tensor* spectroscopy and imaging. *Biophys. J.*, 66:259–267, 1994.

[13] E.L. Bearer, T.L. Falzone, X.W. Zhang, O. Biris, A. Rasin, and R.E. Jacobs. Fole of neuronal activity and kinesin on tract tracing by manganese-enhanced MRI (MEMRI). *Neuroimage*, 37:S37–S46, 2007.

[14] C. Beaulieu. The basis of anisotropic water diffusion in the nervous system – a technical review. *NMR Biomed.*, 15:435–455, 2002.

[15] J.L. Becerra, W.R. Puckett, E.D. Hiester, R.M. Quencer, A.E. Marcillo, M.J.D. Post, and R.P. Bunge. TMR-pathologic comparisons of wallerian degeneration in spinal cord injury. *AJNR Am. J. Neuroradiol.*, 16:125–133, 1995.

[16] S. Bedda, A. Laurent, F. Conti, C. Chéreau, A. Tran, J.T.-V. Nhieu, P. Jaffray, O. Soubrane, C. Goulvestre, Y. Calmus, B. Weill, and F. Batteux. Mangafodipir prevents liver injury induced by acetaminophen in the mouse. *J. Hepatol.*, 39:765–772, 2003.

[17] M.-F. Bellin. MR contrast agents, the old and the new. *Eur. J. of Radiol.*, 60:314–323, 2006.

[18] M.A. Bernstein, K.F. King, and X.J. Zhou. *Handbook of MRI pulse sequences.* Elsevier Academic Press., Burlington, USA, 2004.

[19] M. Berry, J. Carlile, A. Hunter, W. Tsang, P. Rosustrel, and J. Sievers. Optic nerve regeneration after intravitreal peripheral nerve implants: Trajectories of axons regrowing through the optic chiasm into the optic tracts. *J. Neurocytol.*, 28:721–741, 1999.

[20] M. Berry, J. Charlile, and A. Hunter. Peripheral nerve explants grafted into the vitreous body of the eye promote the regeneration of retinal ganglion cell axons severed in the optic nerve. *J. Neurocytol.*, 25:147–170, 1996.

[21] O. Beuf, F. Jaillon, and H. Saint-Jalmes. Small-animal MRI: signal-to-noise ratio comparison at 7 and 1.5 T with multiple-animal acquisition strategies. *Magn. Reson. Mater. Phy.*, 19:202–208, 2006.

[22] D. Le Biham, J. Mangin, C. Poupon, C.A. Clark, S. Pappata, N. Molko, and H. Chabriat. Diffusion tensor imaging: Concepts and applications. *J. Magn. Reson. Imaging*, 13:534–546, 2001.

[23] J.-M. Bonny, P. Mailly, J.-P. Renou, D. Orsal, A. BenMoussa, and O. Stettler. Analysis of laminar activity in normal and injured rat spinal cord by manganese enhanced MRI. *NeuroImage*, 40:1542–1551, 2008.

[24] R.M. Bowler, W. Koller, and P.E. Schulz. Parkinsonism due to manganism in a welder: Neurological and neuropsychological sequalae. *Neurotoxicology*, 27:327–332, 2006.

[25] A.J. Bremerich, M. Saeed, H. Arheden, C.B. Higgins, and M. F. Wendland. Normal and infarcted myocardium: Differentiation with cellular uptake of manganese at MR imaging in a rat model. *Radiology*, 216:524–530, 2000.

[26] E.P. Brouillet, L. Shinobu, U. McGarvey, F. Hochberg, and M.F. Beal. Manganese injection into the rat striatum produces excitotoxic lesions by imparing the energy metabolism. *Exp. Neurol.*, 120:89–94, 1993.

[27] H. Brurok, J.H. Ardenkjær-Larsen, G. Hansson, S. Skarra, K. Berg, J.O.G. Karlsson, I. Laursen, and P. Jynge. Manganese dipyridoxyl diphosphate: MRI contrast agent with antioxidative and cardioprotective properties? *Biochem. Biophys. Res. Commun.*, 254:768–772, 1999.

[28] W.B.J. Cafferty, S.-H. Yang, P.J. Duffy, S. Li, and S.M. Strittmatter. Functional axonal regeneration through astrocytic scar genetically modified to digest chondroitin sulfate proteoglycans. *J. Neurosci.*, 28:2176–2185, 2007.

[29] L. Castelli, F. Tanzi, V. Taglietti, and J. Magistretti. Cu^{2+}, Co^{2+}, and Mn^{2+} modify the gating kinetics of high-voltage-activated Ca^{2+} channels in rat palaeocortical neurons. *J. Membr. Biol.*, 195:121–136, 2003.

[30] C. Cavallotti, D. Cavallotti, N. Pescosolido, and E. Pacella. Age-related changes in rat optic nerve: Morphological studies. *Anat. Histol. Embryol.*, 32:12–16, 2003.

[31] W. O. Cepurna, R. J. Kayton, E. C. Johnson, and J. C. Morrison. Age related optic nerve axonal loss in adult brown norway rats. *Exp. Eye Res.*, 80:877–884, 2005.

[32] K.C. Chan, Q.-L. Fu, E.S. Hui, K.-F. So, and E.X. Wu. Evaluation of the retina and optic nerve in a rat model of chronic glaucoma using in vivo manganese-enhanced magnetic resonance imaging. *Neuroimage*, 40:1166–1174, 2008.

[33] M. Chopp and Y. Li. Treatment of neural injury with marrow stromal cells. *Lancet Neurology*, 1:92–100, 2002.

[34] K.-H. Chuang and A. Koretsky. Improved neuronal tract tracing using manganese enhanced magnetic resonance imaging with fast T_1 mapping. *Magn. Reson. Med.*, 55:604–611, 2006.

[35] D. J. Cross, J. A. Flexman, Y. Anzai, T. J. Morrow, K. R. Maravill, and S. Minoshima. In vivo imaging of functional disruption, recovery and alteration in rat olfactory circuitry after lesion. *NeuroImage*, 32:1265–1272, 2006.

[36] J. Crossgrove and W. Zheng. Manganese toxicity upon overexposure. *NMR Biomed.*, 17:544–553, 2004.

[37] J.S. Crossgrove and R.A. Yokel. Manganese distribution across the blood-brain barrier IV. Evidence for brain influx through store-operated calcium channels. *Neurotoxicology*, 26:297–307, 2005.

[38] S. David and A.J. Aguayo. Axonal elongation into peripheral nervous system "bridges" after central nervous system injury in adult rats. *Science*, 214:931–933, 1981.

[39] S. David and S. Lacroix. Molecular approaches to spinal cord repair. *Annu. Rev. Neurosci.*, 26:411–440, 2003.

[40] S.J.A. Davies, M.T. Fitch, S.P. Memberg, A.K. Hall, G. Raisman, and J. Silver. Regeneration of adult axons in white matter tracts of the central nervous system. *Nature*, 390:680–683, 1997.

[41] M.S. Desole, L. Sciola, M.R. Deloga, S. Sicanca, and R. Migheli. Manganese and 1-methyl-4-(2-ethylphenyl)-1,2,3,6-tetrahydropyridine induce apoptosis in PC12 cells. *Neurosci. Lett.*, 209:193–196, 1996.

[42] T.Q. Doung, A.C. Silva, S. Lee, and S. Kim. Functional MRI of calcium-dependent synaptic activity: cross correlation with CBF and BOLD measurements. *Magn. Reson. Med.*, 43:383–392, 2000.

[43] W.A. Edelstein, G.H Glover, C.J. Hardy, and R.W. Redington. The intrinsic signal-to-noise ratio in NMR imaging. *Magn. Reson. Med.*, 3:604–618, 1986.

[44] R. Eriksson, L. Johansson, T. Bjerner, K. B. Saebo, and H. Ahlstroöm. Uptake of $MnCl_2$ and mangafodipir trisodium in the myocardium: A magnetic resonance imaging study in pigs. *J. Mag. Res. Imaging*, 19:564–569, 2004.

[45] M.J. Firbank, A. Coulthard, R.M. Harrison, and E.D. Williams. A comparison of two methods for measuring the signal to noise ratio on MR images. *Phys. Med. Biol.*, 44:N261–N264, 1999.

[46] K. Fouad, L. Schnell, M.B. Bunge, M.E. Schwab, T. Liebscher, and D.D. Pearse. Combining schwann cell bridges and olfactory-ensheathing glia grafts withchondroitinase promotes locomotor recovery after complete transection of the spinal cord. *J. Neurosci.*, 25:1169–1178, 2005.

[47] Y. Fukunda, M. Watanabe, H. Sawai, and T. Miyoshi. Functional recovery of vision in regenerated optic nerve fibers. *Vision Res.*, 38:1545–1553, 1998.

[48] B. Gallez, C. Baudelet, J. Adline, M. Geurts, and N. Delzenne. Accumulation of manganese in the brain of mice after intravenous injection of manganese-based contrast agents. *Chem. Res. Toxicol.*, 10:360–363, 1997.

[49] D. Garbossa, M. Fontanella, C. Fronda, C. Benevello, G. Muraca, A. Ducati, and A. Vercelli. New strategies for repairing the injured spinal cord: The role of stem cells. *Neurol. Res.*, 28:500–504, 2006.

[50] J.L. Goldberg and B.A. Barres. The relationship between neuronal survival and regeneration. *Annu. Rev. Neurosci.*, 23:579–612, 2000.

[51] E.M. Haacke, R.W. Brown, M.R. Thompson, and R. Venkatesan. *Magnetic resonance imaging. Physical principles and sequence design.* John Wiley & sons, Inc., New York, USA, 1999.

[52] E. Henderson, G. McKinnon, T.-Y. Lee, and B.K. Rutt. A fast 3D Look–Locker method for volumetric T_1 mapping. *Magn. Reson. Imaging*, 17:1163–1171, 1999.

[53] C.C. Huang, N.S. Chu, C.S. Lu, R.S. Chen, and D.B. Calne. Long-term progression in chronic manganism: Ten years of follow-up. *Neurology*, 50:698–700, 1998.

[54] S. Isenmann, A. Kretz, and A. Cellerino. Molecular determinants of retinal ganglion cell development, survival, and regeneration. *Prog. Retinal Eye Res.*, 22:483–543, 2003.

[55] Y. Jiang, X.-A. Mo, F.-Q. Du, X. Fu, X.-Y. Gao, J.-L. Xie, F.-L. Liao, E. Pira, and W. Zheng. Effective treatment of manganese-induced occupational Parkinsonism with p-aminosalicylic acid: A case of 17-year follow-up study. *J. Occuc. Environ. Med*, 48:644–649, 2006.

[56] Y. Jiang, W. Zheng, L. Long, W. Zhao, X. Li, X. Mo, J. Lu, X. Fu, W. Li, S. Liu, Q. Long, J. Huang, and E. Pira. Brain magnetic resonance imaging

and manganese concentrations in red blood cells of smelting workers: Search for biomarkers of manganese exposure. *Neurotoxicology*, 28:126–135, 2007.

[57] K.A. Josephs, J.E. Ahlskog, K.J. Klos, N. Kumar, R.D. Fealey, M.R. Trenerry, and C.T. Cowl. Neurological manifestations in welders with pallidal MRI T_1 hyperintensity. *Neurology*, 64, 2005.

[58] Y.S. Kang, J.C. Gore, and I.M. Armitage. Studies of factors affecting design of NMR contrast agents: Manganese in blood as a model. *Magn. Reson. Med.*, 1:396–409, 1984.

[59] S. Karimi-Abdolrezaee, E. Eftekharpour, J. Wang, C.M. Morshead, and M.G. Fehlings. Delayed transplantation of adult neural precursor cells promotes remyelination and functional neurological recovery after spinal cord injury. *J. Neurosci.*, 26:3377–3389, 2006.

[60] J. Kaslin, J. Ganz, and M. Brand. Proliferation, neurogenesis and regeneration in the non-mammalian vertebrate brain. *Phil. Trans. R. Soc. B*, 363:101–122, 2008.

[61] T. H. Kim, D. H. Yang, J. W . Choi, S. T. Kim, J. H. Yoon, J. H. Shin, J. B. Seo, G. Y. Gong, and T.-H. Lim. Manganese dipyridoxyl diphosphate (MnDPDP)-enhanced magnetic resonance imaging of acute reperfused myocardial injury in a cat model. *Invest. Radiol.*, 40:49–55, 2005.

[62] A. Kristoffersen. Optimal estimation of the diffusion coefficient from non-averaged and averaged noisy magnitude data. *J. Magn. Reson.*, 187:293–305, 2007.

[63] Y. Kuo, A. H. Herlihy, P. So, K.K. Bhakoo, and J.D. Bell. *In vivo* measurements of T_1 relaxation times in mouse brain associated with different modes of systemic administration of manganese chloride. *J. Magn. Reson. Imaging*, 21:334–339, 2005.

[64] B.K. Kwon, C.G. Fisher, M.F. Dvorak, and W. Tetzlaff. Strategies to promote neural repair and regeneration after spinal cord injury. *Spine*, 30:S3–S13, 2005.

[65] R.B. Lauffer. Paramagnetic metal complexed as water proton relaxation agents for NMR imaging: Theory and design. *Chem. Rev.*, 87:901–927, 1987.

[66] P.C. Lauterbur. Image formation by induced local interactions: Examples employing nuclear magnetic resonance. *Nature*, 242:190–191, 1973.

[67] P.C. Lauterbur, M. Mendonca-Dias, and A. Rudin. Augmentation of tissue water proton spin-lattice relaxation rates by in vivo addition of paramag-

netic ions. In P. Dutton, J. S. Leigh, and A. Scarpa, editors, *Frontiers of biological energetics*, pages 752–759. Academic Press, New York, 1978.

[68] Y. Li, P.M. Field, and G. Raisman. Repair of adult rat corticospinal tract by transplants of olfactory ensheathing cells. *Science*, 277:2000–2002, 1997.

[69] Y. Li, Y. Sauvé, D. Li, R.D. Lund, and G. Raisman. Transplanted olfactory ensheathing cells promote regeneration of cut adult rat optic nerve axons. *J. Neurosci.*, 27:7783–7788, 2003.

[70] Linden, A. van der, M. Verhoye, V. Van Meir, I. Tindemans, M. Eens, P. Absil, and J. Balthazart. *In vivo* manganese-enhanced magnetic resonance imaging reveals connections and functional properties of the songbird vocal control system. *Neuroscience*, 112:467–474, 2002.

[71] J.D. Lindsey, M. Scadeng, D.J. Dubowitz, J.G. Crowston, and R.N. Weinreb. Magnetic resonance imaging of the visual system in vivo: Transsynaptic illumination of V1 and V2 visual cortex. *Neuroimage*, 34:1619–1626, 2007.

[72] Y. Liu, H.E. D'Arceuil, S. Westmoreland, J. He, M. Duggan, R.G. Gonzalez, J. Pryor, and A.J. de Crespigny. Serial diffusion tensor MRI after transient and permanent cerebral ischemia in nonhuman primates. *Stroke*, 38:138–145, 2007.

[73] P. Lu and M.H. Tuszynski. Growth factors and combinatorial therapies for CNS regeneration. *Exp. Neurol.*, 209:313–320, 2008.

[74] T. Malaa, L. Aurdal L. Fricha, O. P. Clausen, B. Edwin, O. Soreide, and I. Gladhaug. Intraoperative contrast-enhanced MR-imaging as predictor of tissue damage during cryoablation of porcine liver. *Mag. Res. Imaging*, 21:733–740, 2003.

[75] P. Marzola, F.O. Osculati, and A. Sbarbati. High field MRI in preclinical research. *Eur. J. radiol.*, 48:165–170, 2003.

[76] L. McKerracher. Spinal cord repair: Strategies to promote axon regeneration. *Neurobiol. Dis.*, 8:11–18, 2001.

[77] M.H. Mendonca-Dias, E. Gaggelli, and P.C. Lauterbur. Paramagnetic contrast agents in nuclear magnetic reconance medical imaging. *Semin. Nucl. Med.*, 13:364–376, 1983.

[78] L.D.F. Moon, R.A. Asher, K. E. Rhodes, and J. W. Fawcett. Regeneration of CNS axons back to their target following treatment of adult rat brain with chondroitinase abc. *Nat. Neurosci.*, 4:465–466, 2001.

[79] S. Mori and J. Zhang. Principles of diffusion tensor imaging and its applications to basic neuroscience research. *Neuron*, 51:527–539, 2006.

[80] M.E. Moseley, Y. Cohen, J. Kucharczyk, J. Mintorovitch, , H.S. Asgari, M.F. Wendland, J. Tsuruda, and D. Norman. Diffision-weighted MR imaging of anisotropic water diffusion in cat central nervous system. *Radiology*, 176:439–445, 1990.

[81] J.E. Myers, J. teWaterNaude, M. Fourie, H.B. Abie Zogoe, I. Naik, P. Theodorou, H. Tassel, A. Daya, and M.L. Thompson. Nervous system effects of occupational manganese exposure on South African manganese mineworkers. *Neurotoxicology*, 24:649–656, 2003.

[82] K. Narita, F. Kawasaki, and H. Kita. Mn and Mg influxes through Ca channels of motor nerve terminals are prevented by verapamil in frogs. *Brain Res.*, 510:289–295, 1990.

[83] M.T. Nelson. Interactions of divalent cations with single calcium channels from rat brain synaptosomes. *J. Gen. Physiol.*, 87:201–222, 1986.

[84] W. Nordhøy, H.W. Anthonsen, M. Bruvold, H. Brurok, S. Skarra, J. Krane, and P. Jynge. Intracellular manganese ions provide strong T_1 relaxation in rat myocardium. *Magn. Reson. Med.*, 52:506–514, 2004.

[85] R.B. Norgren and M.N. Lehman. Herpes simplex virus as a transneural tracer. *Neurosci. Biobehav. Rev.*, 22:695–708, 1998.

[86] M. Paques, O. Genevois, A. Régnier, R. Tadayoni, R. Sercombe, A. Gaudric, and E. Vicaut. Axon-tracing properties of indocyanine green. *Arch. Ophthalmol.*, 121:367–370, 2003.

[87] A.M. Parr, C.H. Tator, and A. Keating. Bone marrow-derived mesenchymal stromal cells for the repair of central nervous system injury. *Bone Marrow Transplant.*, 40:606–619, 2007.

[88] R.G. Pautler and A.P. Koretsky. Tracing odor-induced activation in the olfactory bulbs of mice using manganese-enhanced magnetic resonance imaging. *Neuroimage*, 16:441–448, 2002.

[89] R.G. Pautler, R. Mongeau, and R.E. Jacobs. *In vivo* trans-synaptic tract tracing from the murine striatum and amygdala utilizing manganese enhanced MRI (MEMRI). *Magn. Reson. Med.*, 50:33–39, 2003.

[90] R.G. Pautler, A.C. Silva, and A.P. Koretsky. *In vivo* neuronal tract tracing using manganese-enhanced magnetic resonance imaging. *Magn. Reson. Med.*, 40:740–748, 1998.

[91] D. Purves, G.J. Augustine, D. Fitzpatrick, L.C Katz, A.-S. LaMantia, J.O. McNamara, and S.M. Williams, editors. *Neuroscience*. Sinauer, Sunderland, 2000.

[92] G. Raisman. Repair of spinal cord injury by transplantation of olfactory ensheathing cells. *C. R. Biologies*, 330:557–560, 2007.

[93] G. Raisman and Y. Li. Repair of neural pathways by olfactory ensheathing cells. *Nat. Rev. Neurosci.*, 8:312–319, 2006.

[94] S. Ramon y Cajal. *Degeneration and regeneration of the nervous system*. Oxford University Press, London, 1928.

[95] A. Reiner, C.L. Veenman, L. Medina, Y. Jiao, N. Del Mar, and M.G. Honig. Pathway tracing using biotinylated dextran amines. *J. Neurosci. Meth.*, 103:23–37, 2000.

[96] S.M Rocklage, W.P. Cacheris, S.C. Quay, F.E. Hahn, and K.N. Raymond. Manganese(II) N,N'-dipyridoxylethylenediamine-N,N'-diacetate 5,5'-bid(phosphate). Synthesis and characterization of a paramagnetic chelate for magnetic resonance imaging enhancement. *Inorg. Chem*, 28:477–485, 1988.

[97] F. Rovetta, S. Catalani, N. Steimberg, J. Boniotti, M.E. Gilberti, M.A. Mariggiò, and G. Mazzoleni. Organ-specific manganese toxicity: A comparative in vitro study on five models exposed to $MnCl_2$. *Toxicol. In Vitro*, 21:284–292, 2006.

[98] S. Ryu, S.L. Brown, A. Kolozsvary, J.R. Ewing, and J.H. Kim. Noninvasive detection of radiation-induced optic neuropathy by manganese-enhanced MRI. *Radiat. Res.*, 157:500–505, 2002.

[99] N. Sakamoto, K. Kogure, H. Kato, and H. Ohtomo. Disturbed Ca^{2+} homeostasis in the gerbil hippocampus following brief transient ischemia. *Brain Res.*, 364:372–376, 2006.

[100] K.S. Saleem, J.M. Pauls, M. Augath, T. Trinath, B.A. Prause, T. Hashikawa, and N.K. Logothetis. Magnetic resonance imaging of neuronal connections in the macaque monkey. *Neuron*, 34:685–700, 2002.

[101] A. Sandvig, M. Berry, L.B. Barrett, A. Butt, and A. Logan. Myelin-, reactive glia-, and scar-derived CNS axon growth inhibitors: expression, receptor signaling, and correlation with axon regeneration. *Glia*, 46:225–251, 2004.

[102] A. Skjold, B. Amundsen, R. Wiseth, A. Støylen, O. Haraldseth, H.B.W. Larsson, and P. Jynge. Manganese dipyridoxyl-diphosphate (MnDPDP) as

a viability marker in patients with myocardial infarction. *J. Magn. Reson. Imaging*, 26:720–727, 2007.

[103] A. Skjold, T.R. Vandberg, A. Kristoffersen, O. Haraldseth, P. Jynge, and H.B.W. Larsson. Relaxation enhancing properties of MnDPDP in human myocardium. *J. Magn. Reson. Imaging*, 20:948–952, 2004.

[104] W.N. Sloot and J.P. Gramsbergen. Axonal transport of manganese and its relevance to selective neurotoxicity in the rat basal ganglia. *Brain Res.*, 657:124–132, 1994.

[105] S.-K. Song, S.-W. Sun, W.-K. Ju, S.-J-Lin, A.H. Cross, and A.H. Neufeld. Diffusion tensor imaging detects and differentiates axon and myelin degeneration in mouse optic nerve after retinal ischemia. *Neuroimage*, 20:1714–1722, 2003.

[106] S.-K. Song, S.-W. Sun, M.J. Ramsbottom, C. Chang, J. Russel, and A.H. Cross. Dysmyelination revealed through MRI as increased radial (but unchanged axial) diffusion of water. *Neuroimage*, 17:1429–1436, 2002.

[107] D.L. Sparks, L. Lue, T.A. Martin, and J. Rogers. Neural tract tracing using Di-I: A review and a new method to make fast Di-I faster in human brain. *J. Neurosci. Meth.*, 103:3–10, 2000.

[108] B. Stieltjes, S. Klussmann, M. Bock, R. Umathum, J. Mangalathu, E. Letellier, W. Rittgen, L. Edler, P. H. Krammer, H.-U. Kauczor, A. Martin-Villalba, and M. Essig. Manganese-enhanced magnetic resonance imaging for *in vivo* assessment of damage and functional improvement following spinal cord injury in mice. *Mag. Res. Med.*, 55:1124–1131, 2006.

[109] S.-W. Sun, H.-F. Liang, A.H. Cross, and S.-K. Song. Evolving Wallerian degeneration after transient retinal ischemia in mice characterized by diffusion tensor imaging. *Neuroimage*, 40:1–10, 2008.

[110] S.-W. Sun, H.-F. Liang, T. Q. Le, R. C. Armstrong, A. H. Cross, and S.-K. Song. Differential sensitivity of in vivo and ex vivo diffusion tensor imaging to evolving optic nerve injury in mice with retinal ischemia. *Neuroimage*, 32:1195–1204, 2006.

[111] A. Takeda, Y. Kodama, S. Ishiwatari, and S. Okada. Manganese transport in the neural circuit of rat CNS. *Brain Res. Bull.*, 45:149–152, 1998.

[112] C.H. Tator. Review of treatment trials in human spinal cord injury: Issues, difficulties and recommendations. *Neurosurgery.*, 59:957–987, 2006.

[113] Y.D. Teng, E.B Lavik, X. Qu, K.I. Park, J. Ourednik, D. Zurakowski, R. Langer, and E.Y. Snyder. Functional recovery following traumatic spinal

cord injury mediated by a unique polymer scaffold seeded with neural stem cells. *Proc. Natl. Acad. Sci. USA*, 99:3024–3029, 2001.

[114] S. Thanos, R. Naskar, and P. Heiduschka. Regenerating ganglion cell axons in the adult rat establish retinofugal topography and restore visual function. *Exp. Brain Res.*, 114:483–491, 1997.

[115] G. Thomalla, V. Glauche, M.A. Koch, C. Beaulieu, C. Weiller, and J. Röther. Diffusion tensor imaging detects early Wallerian degeneration of the pyramidal tract after ischemic stroke. *Neuroimage*, 22:1767–1774, 2004.

[116] H. Tjälve, J. Henriksson, J. Tallkwist, B.S. Larrson, and N.G. Lindquist. Uptake of manganese and cadmium from the nasal mucosa into the central nervous system via olfactory pathways in rats. *Pharmacol. Toxicol.*, 79:347–356, 1996.

[117] H. Tjälve, C. Mejáre, and K. Borg-Neczak. Uptake and transport of manganese in primary and secondary olfactory neurons in pike. *Pharmacol. Toxicol.*, 77:23–31, 1995.

[118] K.G. Toft, S.O. Hustvedt, D. Grant, I. Martinsen, P.B. Gordon, G.A. Friisk, A.J. Korsmo, and T. Skotland. Metabolism and pharmacokinetics of MnDPDP in man. *Acta Radiol.*, 38:677–689, 1997.

[119] A.W. Toga and R.C. Collins. Metabolic response of optic centers to visual stimuli in the albino rat: Anatomical and physiological considerations. *J. Comp. Neurol.*, 199:443–464, 1981.

[120] J.P. van der Zijden, O. Wu, A. van der Toorn, T. P. Roeling, R.L. Bleys, and R.M. Dijkhuizen. Changes in neuronal connectivity after stroke in rats as studied by serial manganese-enhanced MRI. *Neuroimage*, 34:1650–1657, 2007.

[121] J. Voogd. Visual system. In R. Nieuwenhuys, H.J. Donkelaar, and C. Nicholson, editors, *The central nervous system of vertebrates*, pages 1791–1820. Springer, New York, 1998.

[122] T. Watanabe, J. Frahm, and T. Michaelis. Functional mapping of neural pathways in rodent brain *in vivo* using manganese-enhanced three-dimentional magnetic resonance imaging. *NMR Biomed.*, 17:554–568, 2004.

[123] T. Watanabe, T. Michaelis, and J. Frahm. Mapping of retinal projections in the living rat using high-resolution 3D gradient-echo MRI with Mn^{2+}-induced contrast. *Magn. Reson. Med.*, 46:424–429, 2001.

[124] T. Watanabe, J. Radulovic, J. Spiess, O. Natt, S. Boretius, J. Frahm, and T. Michaelis. *In vivo* 3D MRI staining of the mouse hippocampal system using intracerebral injection of $MnCl_2$. *Neuroimage*, 22:860–867, 2004.

[125] M.F. Wendland. Applications of manganese-enhanced magnetic resonance imaging (MEMRI) to imaging of the heart. *NMR biomed.*, 17:581–594, 2004.

[126] J. Weng, J. Chen, P. Yang, and W.I. Tseng. Functional mapping of rat barrel activation following whisker stimulation using activity-induced manganese-dependent contrast. *Neuroimage*, 36:1179–1188, 2007.

[127] C. Westbrook, C. K. Roth, and J. Talbot, editors. *MRI in practice.* Blackwell Publishing., Oxford, UK, 2005.

[128] C.A.M. Wheeler-Kingshott, G.J.M. Parker, M.R. Syms, S.J. Hickman, P.S. Tofts, D.H. Miller, and G.J. Barker. ADC mapping of the human optic nerve: Increased resolution, coverage, and reliability with CSF-suppressed ZOOM-EPI. *Magn. Reson. Med.*, 47:24–31, 2002.

[129] Q. Wu, H. Butzkueven, M. Gresle, F. Kirchhoff, A. Friedhuber, Q. Yang, H. Wang, K. Fang, H. Lei, G.F. Egan, and T.J. Kilpatrick. MR diffusion changes correlation with ultra-structurally defined axonal degeneration in murine optic nerve. *Neuroimage*, 37:1138–1147, 2007.

[130] S. Zhang, J. Fu, and Z. Zhou. Changes in the brain mitochondrial proteome of male Sprague-Dawley rats treated with manganese chloride. *Toxicol. Appl. Pharmacom.*, 202:13–17, 2005.

[131] S. Zhang, Z. Zhou, and J. Fu. Effect of manganese chloride exposure on liver and brain mitochondria function in rats. *Environ. Res.*, 93:149–157, 2003.

Paper I-IV

Are not included due to copyright

Dissertations at the Faculty of Medicine, NTNU

1977

1. Knut Joachim Berg: EFFECT OF ACETYLSALICYLIC ACID ON RENAL FUNCTION
2. Karl Erik Viken and Arne Ødegaard: STUDIES ON HUMAN MONOCYTES CULTURED *IN VITRO*

1978

3. Karel Bjørn Cyvin: CONGENITAL DISLOCATION OF THE HIP JOINT.
4. Alf O. Brubakk: METHODS FOR STUDYING FLOW DYNAMICS IN THE LEFT VENTRICLE AND THE AORTA IN MAN.

1979

5. Geirmund Unsgaard: CYTOSTATIC AND IMMUNOREGULATORY ABILITIES OF HUMAN BLOOD MONOCYTES CULTURED IN VITRO

1980

6. Størker Jørstad: URAEMIC TOXINS
7. Arne Olav Jenssen: SOME RHEOLOGICAL, CHEMICAL AND STRUCTURAL PROPERTIES OF MUCOID SPUTUM FROM PATIENTS WITH CHRONIC OBSTRUCTIVE BRONCHITIS

1981

8. Jens Hammerstrøm: CYTOSTATIC AND CYTOLYTIC ACTIVITY OF HUMAN MONOCYTES AND EFFUSION MACROPHAGES AGAINST TUMOR CELLS *IN VITRO*

1983

9. Tore Syversen: EFFECTS OF METHYLMERCURY ON RAT BRAIN PROTEIN.
10. Torbjørn Iversen: SQUAMOUS CELL CARCINOMA OF THE VULVA.

1984

11. Tor-Erik Widerøe: ASPECTS OF CONTINUOUS AMBULATORY PERITONEAL DIALYSIS.
12. Anton Hole: ALTERATIONS OF MONOCYTE AND LYMPHOCYTE FUNCTIONS IN REALTION TO SURGERY UNDER EPIDURAL OR GENERAL ANAESTHESIA.
13. Terje Terjesen: FRACTURE HEALING AN STRESS-PROTECTION AFTER METAL PLATE FIXATION AND EXTERNAL FIXATION.
14. Carsten Saunte: CLUSTER HEADACHE SYNDROME.
15. Inggard Lereim: TRAFFIC ACCIDENTS AND THEIR CONSEQUENCES.
16. Bjørn Magne Eggen: STUDIES IN CYTOTOXICITY IN HUMAN ADHERENT MONONUCLEAR BLOOD CELLS.
17. Trond Haug: FACTORS REGULATING BEHAVIORAL EFFECTS OG DRUGS.

1985

18. Sven Erik Gisvold: RESUSCITATION AFTER COMPLETE GLOBAL BRAIN ISCHEMIA.
19. Terje Espevik: THE CYTOSKELETON OF HUMAN MONOCYTES.
20. Lars Bevanger: STUDIES OF THE Ibc (c) PROTEIN ANTIGENS OF GROUP B STREPTOCOCCI.
21. Ole-Jan Iversen: RETROVIRUS-LIKE PARTICLES IN THE PATHOGENESIS OF PSORIASIS.
22. Lasse Eriksen: EVALUATION AND TREATMENT OF ALCOHOL DEPENDENT BEHAVIOUR.
23. Per I. Lundmo: ANDROGEN METABOLISM IN THE PROSTATE.

1986

24. Dagfinn Berntzen: ANALYSIS AND MANAGEMENT OF EXPERIMENTAL AND CLINICAL PAIN.
25. Odd Arnold Kildahl-Andersen: PRODUCTION AND CHARACTERIZATION OF MONOCYTE-DERIVED CYTOTOXIN AND ITS ROLE IN MONOCYTE-MEDIATED CYTOTOXICITY.
26. Ola Dale: VOLATILE ANAESTHETICS.

1987

27. Per Martin Kleveland: STUDIES ON GASTRIN.
28. Audun N. Øksendal: THE CALCIUM PARADOX AND THE HEART.
29. Vilhjalmur R. Finsen: HIP FRACTURES

1988

30. Rigmor Austgulen: TUMOR NECROSIS FACTOR: A MONOCYTE-DERIVED REGULATOR OF CELLULAR GROWTH.
31. Tom-Harald Edna: HEAD INJURIES ADMITTED TO HOSPITAL.

32. Joseph D. Borsi: NEW ASPECTS OF THE CLINICAL PHARMACOKINETICS OF METHOTREXATE.
33. Olav F. M. Sellevold: GLUCOCORTICOIDS IN MYOCARDIAL PROTECTION.
34. Terje Skjærpe: NONINVASIVE QUANTITATION OF GLOBAL PARAMETERS ON LEFT VENTRICULAR FUNCTION: THE SYSTOLIC PULMONARY ARTERY PRESSURE AND CARDIAC OUTPUT.
35. Eyvind Rødahl: STUDIES OF IMMUNE COMPLEXES AND RETROVIRUS-LIKE ANTIGENS IN PATIENTS WITH ANKYLOSING SPONDYLITIS.
36. Ketil Thorstensen: STUDIES ON THE MECHANISMS OF CELLULAR UPTAKE OF IRON FROM TRANSFERRIN.
37. Anna Midelfart: STUDIES OF THE MECHANISMS OF ION AND FLUID TRANSPORT IN THE BOVINE CORNEA.
38. Eirik Helseth: GROWTH AND PLASMINOGEN ACTIVATOR ACTIVITY OF HUMAN GLIOMAS AND BRAIN METASTASES - WITH SPECIAL REFERENCE TO TRANSFORMING GROWTH FACTOR BETA AND THE EPIDERMAL GROWTH FACTOR RECEPTOR.
39. Petter C. Borchgrevink: MAGNESIUM AND THE ISCHEMIC HEART.
40. Kjell-Arne Rein: THE EFFECT OF EXTRACORPOREAL CIRCULATION ON SUBCUTANEOUS TRANSCAPILLARY FLUID BALANCE.
41. Arne Kristian Sandvik: RAT GASTRIC HISTAMINE.
42. Carl Bredo Dahl: ANIMAL MODELS IN PSYCHIATRY.

1989

43. Torbjørn A. Fredriksen: CERVICOGENIC HEADACHE.
44. Rolf A. Walstad: CEFTAZIDIME.
45. Rolf Salvesen: THE PUPIL IN CLUSTER HEADACHE.
46. Nils Petter Jørgensen: DRUG EXPOSURE IN EARLY PREGNANCY.
47. Johan C. Ræder: PREMEDICATION AND GENERAL ANAESTHESIA IN OUTPATIENT GYNECOLOGICAL SURGERY.
48. M. R. Shalaby: IMMUNOREGULATORY PROPERTIES OF TNF-α AND THE RELATED CYTOKINES.
49. Anders Waage: THE COMPLEX PATTERN OF CYTOKINES IN SEPTIC SHOCK.
50. Bjarne Christian Eriksen: ELECTROSTIMULATION OF THE PELVIC FLOOR IN FEMALE URINARY INCONTINENCE.
51. Tore B. Halvorsen: PROGNOSTIC FACTORS IN COLORECTAL CANCER.

1990

52. Asbjørn Nordby: CELLULAR TOXICITY OF ROENTGEN CONTRAST MEDIA.
53. Kåre E. Tvedt: X-RAY MICROANALYSIS OF BIOLOGICAL MATERIAL.
54. Tore C. Stiles: COGNITIVE VULNERABILITY FACTORS IN THE DEVELOPMENT AND MAINTENANCE OF DEPRESSION.
55. Eva Hofsli: TUMOR NECROSIS FACTOR AND MULTIDRUG RESISTANCE.
56. Helge S. Haarstad: TROPHIC EFFECTS OF CHOLECYSTOKININ AND SECRETIN ON THE RAT PANCREAS.
57. Lars Engebretsen: TREATMENT OF ACUTE ANTERIOR CRUCIATE LIGAMENT INJURIES.
58. Tarjei Rygnestad: DELIBERATE SELF-POISONING IN TRONDHEIM.
59. Arne Z. Henriksen: STUDIES ON CONSERVED ANTIGENIC DOMAINS ON MAJOR OUTER MEMBRANE PROTEINS FROM ENTEROBACTERIA.
60. Steinar Westin: UNEMPLOYMENT AND HEALTH: Medical and social consequences of a factory closure in a ten-year controlled follow-up study.
61. Ylva Sahlin: INJURY REGISTRATION, a tool for accident preventive work.
62. Helge Bjørnstad Pettersen: BIOSYNTHESIS OF COMPLEMENT BY HUMAN ALVEOLAR MACROPHAGES WITH SPECIAL REFERENCE TO SARCOIDOSIS.
63. Berit Schei: TRAPPED IN PAINFUL LOVE.
64. Lars J. Vatten: PROSPECTIVE STUDIES OF THE RISK OF BREAST CANCER IN A COHORT OF NORWEGIAN WOMAN.

1991

65. Kåre Bergh: APPLICATIONS OF ANTI-C5a SPECIFIC MONOCLONAL ANTIBODIES FOR THE ASSESSMENT OF COMPLEMENT ACTIVATION.
66. Svein Svenningsen: THE CLINICAL SIGNIFICANCE OF INCREASED FEMORAL ANTEVERSION.

67. Olbjørn Klepp: NONSEMINOMATOUS GERM CELL TESTIS CANCER: THERAPEUTIC OUTCOME AND PROGNOSTIC FACTORS.
68. Trond Sand: THE EFFECTS OF CLICK POLARITY ON BRAINSTEM AUDITORY EVOKED POTENTIALS AMPLITUDE, DISPERSION, AND LATENCY VARIABLES.
69. Kjetil B. Åsbakk: STUDIES OF A PROTEIN FROM PSORIATIC SCALE, PSO P27, WITH RESPECT TO ITS POTENTIAL ROLE IN IMMUNE REACTIONS IN PSORIASIS.
70. Arnulf Hestnes: STUDIES ON DOWN´S SYNDROME.
71. Randi Nygaard: LONG-TERM SURVIVAL IN CHILDHOOD LEUKEMIA.
72. Bjørn Hagen: THIO-TEPA.
73. Svein Anda: EVALUATION OF THE HIP JOINT BY COMPUTED TOMOGRAMPHY AND ULTRASONOGRAPHY.

1992

74. Martin Svartberg: AN INVESTIGATION OF PROCESS AND OUTCOME OF SHORT-TERM PSYCHODYNAMIC PSYCHOTHERAPY.
75. Stig Arild Slørdahl: AORTIC REGURGITATION.
76. Harold C Sexton: STUDIES RELATING TO THE TREATMENT OF SYMPTOMATIC NON-PSYCHOTIC PATIENTS.
77. Maurice B. Vincent: VASOACTIVE PEPTIDES IN THE OCULAR/FOREHEAD AREA.
78. Terje Johannessen: CONTROLLED TRIALS IN SINGLE SUBJECTS.
79. Turid Nilsen: PYROPHOSPHATE IN HEPATOCYTE IRON METABOLISM.
80. Olav Haraldseth: NMR SPECTROSCOPY OF CEREBRAL ISCHEMIA AND REPERFUSION IN RAT.
81. Eiliv Brenna: REGULATION OF FUNCTION AND GROWTH OF THE OXYNTIC MUCOSA.

1993

82. Gunnar Bovim: CERVICOGENIC HEADACHE.
83. Jarl Arne Kahn: ASSISTED PROCREATION.
84. Bjørn Naume: IMMUNOREGULATORY EFFECTS OF CYTOKINES ON NK CELLS.
85. Rune Wiseth: AORTIC VALVE REPLACEMENT.
86. Jie Ming Shen: BLOOD FLOW VELOCITY AND RESPIRATORY STUDIES.
87. Piotr Kruszewski: SUNCT SYNDROME WITH SPECIAL REFERENCE TO THE AUTONOMIC NERVOUS SYSTEM.
88. Mette Haase Moen: ENDOMETRIOSIS.
89. Anne Vik: VASCULAR GAS EMBOLISM DURING AIR INFUSION AND AFTER DECOMPRESSION IN PIGS.
90. Lars Jacob Stovner: THE CHIARI TYPE I MALFORMATION.
91. Kjell Å. Salvesen: ROUTINE ULTRASONOGRAPHY IN UTERO AND DEVELOPMENT IN CHILDHOOD.

1994

92. Nina-Beate Liabakk: DEVELOPMENT OF IMMUNOASSAYS FOR TNF AND ITS SOLUBLE RECEPTORS.
93. Sverre Helge Torp: *erb*B ONCOGENES IN HUMAN GLIOMAS AND MENINGIOMAS.
94. Olav M. Linaker: MENTAL RETARDATION AND PSYCHIATRY. Past and present.
95. Per Oscar Feet: INCREASED ANTIDEPRESSANT AND ANTIPANIC EFFECT IN COMBINED TREATMENT WITH DIXYRAZINE AND TRICYCLIC ANTIDEPRESSANTS.
96. Stein Olav Samstad: CROSS SECTIONAL FLOW VELOCITY PROFILES FROM TWO-DIMENSIONAL DOPPLER ULTRASOUND: Studies on early mitral blood flow.
97. Bjørn Backe: STUDIES IN ANTENATAL CARE.
98. Gerd Inger Ringdal: QUALITY OF LIFE IN CANCER PATIENTS.
99. Torvid Kiserud: THE DUCTUS VENOSUS IN THE HUMAN FETUS.
100. Hans E. Fjøsne: HORMONAL REGULATION OF PROSTATIC METABOLISM.
101. Eylert Brodtkorb: CLINICAL ASPECTS OF EPILEPSY IN THE MENTALLY RETARDED.
102. Roar Juul: PEPTIDERGIC MECHANISMS IN HUMAN SUBARACHNOID HEMORRHAGE.
103. Unni Syversen: CHROMOGRANIN A. Phsysiological and Clinical Role.

1995

104. Odd Gunnar Brakstad: THERMOSTABLE NUCLEASE AND THE *nuc* GENE IN THE DIAGNOSIS OF *Staphylococcus aureus* INFECTIONS.
105. Terje Engan: NUCLEAR MAGNETIC RESONANCE (NMR) SPECTROSCOPY OF PLASMA IN MALIGNANT DISEASE.
106. Kirsten Rasmussen: VIOLENCE IN THE MENTALLY DISORDERED.
107. Finn Egil Skjeldestad: INDUCED ABORTION: Timetrends and Determinants.

108. Roar Stenseth: THORACIC EPIDURAL ANALGESIA IN AORTOCORONARY BYPASS SURGERY.
109. Arild Faxvaag: STUDIES OF IMMUNE CELL FUNCTION *in mice infected with* MURINE RETROVIRUS.

1996

110. Svend Aakhus: NONINVASIVE COMPUTERIZED ASSESSMENT OF LEFT VENTRICULAR FUNCTION AND SYSTEMIC ARTERIAL PROPERTIES. Methodology and some clinical applications.
111. Klaus-Dieter Bolz: INTRAVASCULAR ULTRASONOGRAPHY.
112. Petter Aadahl: CARDIOVASCULAR EFFECTS OF THORACIC AORTIC CROSS-CLAMPING.
113. Sigurd Steinshamn: CYTOKINE MEDIATORS DURING GRANULOCYTOPENIC INFECTIONS.
114. Hans Stifoss-Hanssen: SEEKING MEANING OR HAPPINESS?
115. Anne Kvikstad: LIFE CHANGE EVENTS AND MARITAL STATUS IN RELATION TO RISK AND PROGNOSIS OF CANSER.
116. Torbjørn Grøntvedt: TREATMENT OF ACUTE AND CHRONIC ANTERIOR CRUCIATE LIGAMENT INJURIES. A clinical and biomechanical study.
117. Sigrid Hørven Wigers: CLINICAL STUDIES OF FIBROMYALGIA WITH FOCUS ON ETIOLOGY, TREATMENT AND OUTCOME.
118. Jan Schjøtt: MYOCARDIAL PROTECTION: Functional and Metabolic Characteristics of Two Endogenous Protective Principles.
119. Marit Martinussen: STUDIES OF INTESTINAL BLOOD FLOW AND ITS RELATION TO TRANSITIONAL CIRCULATORY ADAPATION IN NEWBORN INFANTS.
120. Tomm B. Müller: MAGNETIC RESONANCE IMAGING IN FOCAL CEREBRAL ISCHEMIA.
121. Rune Haaverstad: OEDEMA FORMATION OF THE LOWER EXTREMITIES.
122. Magne Børset: THE ROLE OF CYTOKINES IN MULTIPLE MYELOMA, WITH SPECIAL REFERENCE TO HEPATOCYTE GROWTH FACTOR.
123. Geir Smedslund: A THEORETICAL AND EMPIRICAL INVESTIGATION OF SMOKING, STRESS AND DISEASE: RESULTS FROM A POPULATION SURVEY.

1997

124. Torstein Vik: GROWTH, MORBIDITY, AND PSYCHOMOTOR DEVELOPMENT IN INFANTS WHO WERE GROWTH RETARDED *IN UTERO*.
125. Siri Forsmo: ASPECTS AND CONSEQUENCES OF OPPORTUNISTIC SCREENING FOR CERVICAL CANCER. Results based on data from three Norwegian counties.
126. Jon S. Skranes: CEREBRAL MRI AND NEURODEVELOPMENTAL OUTCOME IN VERY LOW BIRTH WEIGHT (VLBW) CHILDREN. A follow-up study of a geographically based year cohort of VLBW children at ages one and six years.
127. Knut Bjørnstad: COMPUTERIZED ECHOCARDIOGRAPHY FOR EVALUTION OF CORONARY ARTERY DISEASE.
128. Grethe Elisabeth Borchgrevink: DIAGNOSIS AND TREATMENT OF WHIPLASH/NECK SPRAIN INJURIES CAUSED BY CAR ACCIDENTS.
129. Tor Elsås: NEUROPEPTIDES AND NITRIC OXIDE SYNTHASE IN OCULAR AUTONOMIC AND SENSORY NERVES.
130. Rolf W. Gråwe: EPIDEMIOLOGICAL AND NEUROPSYCHOLOGICAL PERSPECTIVES ON SCHIZOPHRENIA.
131. Tonje Strømholm: CEREBRAL HAEMODYNAMICS DURING THORACIC AORTIC CROSSCLAMPING. An experimental study in pigs.

1998

132. Martinus Bråten: STUDIES ON SOME PROBLEMS REALTED TO INTRAMEDULLARY NAILING OF FEMORAL FRACTURES.
133. Ståle Nordgård: PROLIFERATIVE ACTIVITY AND DNA CONTENT AS PROGNOSTIC INDICATORS IN ADENOID CYSTIC CARCINOMA OF THE HEAD AND NECK.
134. Egil Lien: SOLUBLE RECEPTORS FOR **TNF** AND **LPS**: RELEASE PATTERN AND POSSIBLE SIGNIFICANCE IN DISEASE.
135. Marit Bjørgaas: HYPOGLYCAEMIA IN CHILDREN WITH DIABETES MELLITUS
136. Frank Skorpen: GENETIC AND FUNCTIONAL ANALYSES OF DNA REPAIR IN HUMAN CELLS.
137. Juan A. Pareja: SUNCT SYNDROME. ON THE CLINICAL PICTURE. ITS DISTINCTION FROM OTHER, SIMILAR HEADACHES.

138. Anders Angelsen: NEUROENDOCRINE CELLS IN HUMAN PROSTATIC CARCINOMAS AND THE PROSTATIC COMPLEX OF RAT, GUINEA PIG, CAT AND DOG.
139. Fabio Antonaci: CHRONIC PAROXYSMAL HEMICRANIA AND HEMICRANIA CONTINUA: TWO DIFFERENT ENTITIES?
140. Sven M. Carlsen: ENDOCRINE AND METABOLIC EFFECTS OF METFORMIN WITH SPECIAL EMPHASIS ON CARDIOVASCULAR RISK FACTORES.

1999

141. Terje A. Murberg: DEPRESSIVE SYMPTOMS AND COPING AMONG PATIENTS WITH CONGESTIVE HEART FAILURE.
142. Harm-Gerd Karl Blaas: THE EMBRYONIC EXAMINATION. Ultrasound studies on the development of the human embryo.
143. Noèmi Becser Andersen:THE CEPHALIC SENSORY NERVES IN UNILATERAL HEADACHES. Anatomical background and neurophysiological evaluation.
144. Eli-Janne Fiskerstrand: LASER TREATMENT OF PORT WINE STAINS. A study of the efficacy and limitations of the pulsed dye laser. Clinical and morfological analyses aimed at improving the therapeutic outcome.
145. Bård Kulseng: A STUDY OF ALGINATE CAPSULE PROPERTIES AND CYTOKINES IN RELATION TO INSULIN DEPENDENT DIABETES MELLITUS.
146. Terje Haug: STRUCTURE AND REGULATION OF THE HUMAN UNG GENE ENCODING URACIL-DNA GLYCOSYLASE.
147. Heidi Brurok: MANGANESE AND THE HEART. A Magic Metal with Diagnostic and Therapeutic Possibilites.
148. Agnes Kathrine Lie: DIAGNOSIS AND PREVALENCE OF HUMAN PAPILLOMAVIRUS INFECTION IN CERVICAL INTRAEPITELIAL NEOPLASIA. Relationship to Cell Cycle Regulatory Proteins and HLA DQBI Genes.
149. Ronald Mårvik: PHARMACOLOGICAL, PHYSIOLOGICAL AND PATHOPHYSIOLOGICAL STUDIES ON ISOLATED STOMACS.
150. Ketil Jarl Holen: THE ROLE OF ULTRASONOGRAPHY IN THE DIAGNOSIS AND TREATMENT OF HIP DYSPLASIA IN NEWBORNS.
151. Irene Hetlevik: THE ROLE OF CLINICAL GUIDELINES IN CARDIOVASCULAR RISK INTERVENTION IN GENERAL PRACTICE.
152. Katarina Tunòn: ULTRASOUND AND PREDICTION OF GESTATIONAL AGE.
153. Johannes Soma: INTERACTION BETWEEN THE LEFT VENTRICLE AND THE SYSTEMIC ARTERIES.
154. Arild Aamodt: DEVELOPMENT AND PRE-CLINICAL EVALUATION OF A CUSTOM-MADE FEMORAL STEM.
155. Agnar Tegnander: DIAGNOSIS AND FOLLOW-UP OF CHILDREN WITH SUSPECTED OR KNOWN HIP DYSPLASIA.
156. Bent Indredavik: STROKE UNIT TREATMENT: SHORT AND LONG-TERM EFFECTS
157. Jolanta Vanagaite Vingen: PHOTOPHOBIA AND PHONOPHOBIA IN PRIMARY HEADACHES

2000

158. Ola Dalsegg Sæther: PATHOPHYSIOLOGY DURING PROXIMAL AORTIC CROSS-CLAMPING CLINICAL AND EXPERIMENTAL STUDIES
159. xxxxxxxxx (blind number)
160. Christina Vogt Isaksen: PRENATAL ULTRASOUND AND POSTMORTEM FINDINGS – A TEN YEAR CORRELATIVE STUDY OF FETUSES AND INFANTS WITH DEVELOPMENTAL ANOMALIES.
161. Holger Seidel: HIGH-DOSE METHOTREXATE THERAPY IN CHILDREN WITH ACUTE LYMPHOCYTIC LEUKEMIA: DOSE, CONCENTRATION, AND EFFECT CONSIDERATIONS.
162. Stein Hallan: IMPLEMENTATION OF MODERN MEDICAL DECISION ANALYSIS INTO CLINICAL DIAGNOSIS AND TREATMENT.
163. Malcolm Sue-Chu: INVASIVE AND NON-INVASIVE STUDIES IN CROSS-COUNTRY SKIERS WITH ASTHMA-LIKE SYMPTOMS.
164. Ole-Lars Brekke: EFFECTS OF ANTIOXIDANTS AND FATTY ACIDS ON TUMOR NECROSIS FACTOR-INDUCED CYTOTOXICITY.
165. Jan Lundbom: AORTOCORONARY BYPASS SURGERY: CLINICAL ASPECTS, COST CONSIDERATIONS AND WORKING ABILITY.

166. John-Anker Zwart: LUMBAR NERVE ROOT COMPRESSION, BIOCHEMICAL AND NEUROPHYSIOLOGICAL ASPECTS.
167. Geir Falck: HYPEROSMOLALITY AND THE HEART.
168. Eirik Skogvoll: CARDIAC ARREST Incidence, Intervention and Outcome.
169. Dalius Bansevicius: SHOULDER-NECK REGION IN CERTAIN HEADACHES AND CHRONIC PAIN SYNDROMES.
170. Bettina Kinge: REFRACTIVE ERRORS AND BIOMETRIC CHANGES AMONG UNIVERSITY STUDENTS IN NORWAY.
171. Gunnar Qvigstad: CONSEQUENCES OF HYPERGASTRINEMIA IN MAN
172. Hanne Ellekjær: EPIDEMIOLOGICAL STUDIES OF STROKE IN A NORWEGIAN POPULATION. INCIDENCE, RISK FACTORS AND PROGNOSIS
173. Hilde Grimstad: VIOLENCE AGAINST WOMEN AND PREGNANCY OUTCOME.
174. Astrid Hjelde: SURFACE TENSION AND COMPLEMENT ACTIVATION: Factors influencing bubble formation and bubble effects after decompression.
175. Kjell A. Kvistad: MR IN BREAST CANCER – A CLINICAL STUDY.
176. Ivar Rossvoll: ELECTIVE ORTHOPAEDIC SURGERY IN A DEFINED POPULATION. Studies on demand, waiting time for treatment and incapacity for work.
177. Carina Seidel: PROGNOSTIC VALUE AND BIOLOGICAL EFFECTS OF HEPATOCYTE GROWTH FACTOR AND SYNDECAN-1 IN MULTIPLE MYELOMA.

2001

178. Alexander Wahba: THE INFLUENCE OF CARDIOPULMONARY BYPASS ON PLATELET FUNCTION AND BLOOD COAGULATION – DETERMINANTS AND CLINICAL CONSEQUENSES
179. Marcus Schmitt-Egenolf: THE RELEVANCE OF THE MAJOR hISTOCOMPATIBILITY COMPLEX FOR THE GENETICS OF PSORIASIS
180. Odrun Arna Gederaas: BIOLOGICAL MECHANISMS INVOLVED IN 5-AMINOLEVULINIC ACID BASED PHOTODYNAMIC THERAPY
181. Pål Richard Romundstad: CANCER INCIDENCE AMONG NORWEGIAN ALUMINIUM WORKERS
182. Henrik Hjorth-Hansen: NOVEL CYTOKINES IN GROWTH CONTROL AND BONE DISEASE OF MULTIPLE MYELOMA
183. Gunnar Morken: SEASONAL VARIATION OF HUMAN MOOD AND BEHAVIOUR
184. Bjørn Olav Haugen: MEASUREMENT OF CARDIAC OUTPUT AND STUDIES OF VELOCITY PROFILES IN AORTIC AND MITRAL FLOW USING TWO- AND THREE-DIMENSIONAL COLOUR FLOW IMAGING
185. Geir Bråthen: THE CLASSIFICATION AND CLINICAL DIAGNOSIS OF ALCOHOL-RELATED SEIZURES
186. Knut Ivar Aasarød: RENAL INVOLVEMENT IN INFLAMMATORY RHEUMATIC DISEASE. A Study of Renal Disease in Wegener's Granulomatosis and in Primary Sjögren's Syndrome
187. Trude Helen Flo: RESEPTORS INVOLVED IN CELL ACTIVATION BY DEFINED URONIC ACID POLYMERS AND BACTERIAL COMPONENTS
188. Bodil Kavli: HUMAN URACIL-DNA GLYCOSYLASES FROM THE UNG GENE: STRUCTRUAL BASIS FOR SUBSTRATE SPECIFICITY AND REPAIR
189. Liv Thommesen: MOLECULAR MECHANISMS INVOLVED IN TNF- AND GASTRIN-MEDIATED GENE REGULATION
190. Turid Lingaas Holmen: SMOKING AND HEALTH IN ADOLESCENCE; THE NORD-TRØNDELAG HEALTH STUDY, 1995-97
191. Øyvind Hjertner: MULTIPLE MYELOMA: INTERACTIONS BETWEEN MALIGNANT PLASMA CELLS AND THE BONE MICROENVIRONMENT
192. Asbjørn Støylen: STRAIN RATE IMAGING OF THE LEFT VENTRICLE BY ULTRASOUND. FEASIBILITY, CLINICAL VALIDATION AND PHYSIOLOGICAL ASPECTS
193. Kristian Midthjell: DIABETES IN ADULTS IN NORD-TRØNDELAG. PUBLIC HEALTH ASPECTS OF DIABETES MELLITUS IN A LARGE, NON-SELECTED NORWEGIAN POPULATION.
194. Guanglin Cui: FUNCTIONAL ASPECTS OF THE ECL CELL IN RODENTS
195. Ulrik Wisløff: CARDIAC EFFECTS OF AEROBIC ENDURANCE TRAINING: HYPERTROPHY, CONTRACTILITY AND CALCUIM HANDLING IN NORMAL AND FAILING HEART
196. Øyvind Halaas: MECHANISMS OF IMMUNOMODULATION AND CELL-MEDIATED CYTOTOXICITY INDUCED BY BACTERIAL PRODUCTS

197. Tore Amundsen: PERFUSION MR IMAGING IN THE DIAGNOSIS OF PULMONARY EMBOLISM
198. Nanna Kurtze: THE SIGNIFICANCE OF ANXIETY AND DEPRESSION IN FATIQUE AND PATTERNS OF PAIN AMONG INDIVIDUALS DIAGNOSED WITH FIBROMYALGIA: RELATIONS WITH QUALITY OF LIFE, FUNCTIONAL DISABILITY, LIFESTYLE, EMPLOYMENT STATUS, CO-MORBIDITY AND GENDER
199. Tom Ivar Lund Nilsen: PROSPECTIVE STUDIES OF CANCER RISK IN NORD-TRØNDELAG: THE HUNT STUDY. Associations with anthropometric, socioeconomic, and lifestyle risk factors
200. Asta Kristine Håberg: A NEW APPROACH TO THE STUDY OF MIDDLE CEREBRAL ARTERY OCCLUSION IN THE RAT USING MAGNETIC RESONANCE TECHNIQUES

2002

201. Knut Jørgen Arntzen: PREGNANCY AND CYTOKINES
202. Henrik Døllner: INFLAMMATORY MEDIATORS IN PERINATAL INFECTIONS
203. Asta Bye: LOW FAT, LOW LACTOSE DIET USED AS PROPHYLACTIC TREATMENT OF ACUTE INTESTINAL REACTIONS DURING PELVIC RADIOTHERAPY. A PROSPECTIVE RANDOMISED STUDY.
204. Sylvester Moyo: STUDIES ON STREPTOCOCCUS AGALACTIAE (GROUP B STREPTOCOCCUS) SURFACE-ANCHORED MARKERS WITH EMPHASIS ON STRAINS AND HUMAN SERA FROM ZIMBABWE.
205. Knut Hagen: HEAD-HUNT: THE EPIDEMIOLOGY OF HEADACHE IN NORD-TRØNDELAG
206. Li Lixin: ON THE REGULATION AND ROLE OF UNCOUPLING PROTEIN-2 IN INSULIN PRODUCING ß-CELLS
207. Anne Hildur Henriksen: SYMPTOMS OF ALLERGY AND ASTHMA VERSUS MARKERS OF LOWER AIRWAY INFLAMMATION AMONG ADOLESCENTS
208. Egil Andreas Fors: NON-MALIGNANT PAIN IN RELATION TO PSYCHOLOGICAL AND ENVIRONTENTAL FACTORS. EXPERIENTAL AND CLINICAL STUDES OF PAIN WITH FOCUS ON FIBROMYALGIA
209. Pål Klepstad: MORPHINE FOR CANCER PAIN
210. Ingunn Bakke: MECHANISMS AND CONSEQUENCES OF PEROXISOME PROLIFERATOR-INDUCED HYPERFUNCTION OF THE RAT GASTRIN PRODUCING CELL
211. Ingrid Susann Gribbestad: MAGNETIC RESONANCE IMAGING AND SPECTROSCOPY OF BREAST CANCER
212. Rønnaug Astri Ødegård: PREECLAMPSIA – MATERNAL RISK FACTORS AND FETAL GROWTH
213. Johan Haux: STUDIES ON CYTOTOXICITY INDUCED BY HUMAN NATURAL KILLER CELLS AND DIGITOXIN
214. Turid Suzanne Berg-Nielsen: PARENTING PRACTICES AND MENTALLY DISORDERED ADOLESCENTS
215. Astrid Rydning: BLOOD FLOW AS A PROTECTIVE FACTOR FOR THE STOMACH MUCOSA. AN EXPERIMENTAL STUDY ON THE ROLE OF MAST CELLS AND SENSORY AFFERENT NEURONS

2003

216. Jan Pål Loennechen: HEART FAILURE AFTER MYOCARDIAL INFARCTION. Regional Differences, Myocyte Function, Gene Expression, and Response to Cariporide, Losartan, and Exercise Training.
217. Elisabeth Qvigstad: EFFECTS OF FATTY ACIDS AND OVER-STIMULATION ON INSULIN SECRETION IN MAN
218. Arne Åsberg: EPIDEMIOLOGICAL STUDIES IN HEREDITARY HEMOCHROMATOSIS: PREVALENCE, MORBIDITY AND BENEFIT OF SCREENING.
219. Johan Fredrik Skomsvoll: REPRODUCTIVE OUTCOME IN WOMEN WITH RHEUMATIC DISEASE. A population registry based study of the effects of inflammatory rheumatic disease and connective tissue disease on reproductive outcome in Norwegian women in 1967-1995.
220. Siv Mørkved: URINARY INCONTINENCE DURING PREGNANCY AND AFTER DELIVERY: EFFECT OF PELVIC FLOOR MUSCLE TRAINING IN PREVENTION AND TREATMENT
221. Marit S. Jordhøy: THE IMPACT OF COMPREHENSIVE PALLIATIVE CARE
222. Tom Christian Martinsen: HYPERGASTRINEMIA AND HYPOACIDITY IN RODENTS – CAUSES AND CONSEQUENCES

223. Solveig Tingulstad: CENTRALIZATION OF PRIMARY SURGERY FOR OVARAIN CANCER. FEASIBILITY AND IMPACT ON SURVIVAL
224. Haytham Eloqayli: METABOLIC CHANGES IN THE BRAIN CAUSED BY EPILEPTIC SEIZURES
225. Torunn Bruland: STUDIES OF EARLY RETROVIRUS-HOST INTERACTIONS – VIRAL DETERMINANTS FOR PATHOGENESIS AND THE INFLUENCE OF SEX ON THE SUSCEPTIBILITY TO FRIEND MURINE LEUKAEMIA VIRUS INFECTION
226. Torstein Hole: DOPPLER ECHOCARDIOGRAPHIC EVALUATION OF LEFT VENTRICULAR FUNCTION IN PATIENTS WITH ACUTE MYOCARDIAL INFARCTION
227. Vibeke Nossum: THE EFFECT OF VASCULAR BUBBLES ON ENDOTHELIAL FUNCTION
228. Sigurd Fasting: ROUTINE BASED RECORDING OF ADVERSE EVENTS DURING ANAESTHESIA – APPLICATION IN QUALITY IMPROVEMENT AND SAFETY
229. Solfrid Romundstad: EPIDEMIOLOGICAL STUDIES OF MICROALBUMINURIA. THE NORD-TRØNDELAG HEALTH STUDY 1995-97 (HUNT 2)
230. Geir Torheim: PROCESSING OF DYNAMIC DATA SETS IN MAGNETIC RESONANCE IMAGING
231. Catrine Ahlén: SKIN INFECTIONS IN OCCUPATIONAL SATURATION DIVERS IN THE NORTH SEA AND THE IMPACT OF THE ENVIRONMENT
232. Arnulf Langhammer: RESPIRATORY SYMPTOMS, LUNG FUNCTION AND BONE MINERAL DENSITY IN A COMPREHENSIVE POPULATION SURVEY. THE NORD-TRØNDELAG HEALTH STUDY 1995-97. THE BRONCHIAL OBSTRUCTION IN NORD-TRØNDELAG STUDY
233. Einar Kjelsås: EATING DISORDERS AND PHYSICAL ACTIVITY IN NON-CLINICAL SAMPLES
234. Arne Wibe: RECTAL CANCER TREATMENT IN NORWAY – STANDARDISATION OF SURGERY AND QUALITY ASSURANCE

2004

235. Eivind Witsø: BONE GRAFT AS AN ANTIBIOTIC CARRIER
236. Anne Mari Sund: DEVELOPMENT OF DEPRESSIVE SYMPTOMS IN EARLY ADOLESCENCE
237. Hallvard Lærum: EVALUATION OF ELECTRONIC MEDICAL RECORDS – A CLINICAL TASK PERSPECTIVE
238. Gustav Mikkelsen: ACCESSIBILITY OF INFORMATION IN ELECTRONIC PATIENT RECORDS; AN EVALUATION OF THE ROLE OF DATA QUALITY
239. Steinar Krokstad: SOCIOECONOMIC INEQUALITIES IN HEALTH AND DISABILITY. SOCIAL EPIDEMIOLOGY IN THE NORD-TRØNDELAG HEALTH STUDY (HUNT), NORWAY
240. Arne Kristian Myhre: NORMAL VARIATION IN ANOGENITAL ANATOMY AND MICROBIOLOGY IN NON-ABUSED PRESCHOOL CHILDREN
241. Ingunn Dybedal: NEGATIVE REGULATORS OF HEMATOPOIETEC STEM AND PROGENITOR CELLS
242. Beate Sitter: TISSUE CHARACTERIZATION BY HIGH RESOLUTION MAGIC ANGLE SPINNING MR SPECTROSCOPY
243. Per Arne Aas: MACROMOLECULAR MAINTENANCE IN HUMAN CELLS – REPAIR OF URACIL IN DNA AND METHYLATIONS IN DNA AND RNA
244. Anna Bofin: FINE NEEDLE ASPIRATION CYTOLOGY IN THE PRIMARY INVESTIGATION OF BREAST TUMOURS AND IN THE DETERMINATION OF TREATMENT STRATEGIES
245. Jim Aage Nøttestad: DEINSTITUTIONALIZATION AND MENTAL HEALTH CHANGES AMONG PEOPLE WITH MENTAL RETARDATION
246. Reidar Fossmark: GASTRIC CANCER IN JAPANESE COTTON RATS
247. Wibeke Nordhøy: MANGANESE AND THE HEART, INTRACELLULAR MR RELAXATION AND WATER EXCHANGE ACROSS THE CARDIAC CELL MEMBRANE

2005

248. Sturla Molden: QUANTITATIVE ANALYSES OF SINGLE UNITS RECORDED FROM THE HIPPOCAMPUS AND ENTORHINAL CORTEX OF BEHAVING RATS
249. Wenche Brenne Drøyvold: EPIDEMIOLOGICAL STUDIES ON WEIGHT CHANGE AND HEALTH IN A LARGE POPULATION. THE NORD-TRØNDELAG HEALTH STUDY (HUNT)

250. Ragnhild Støen: ENDOTHELIUM-DEPENDENT VASODILATION IN THE FEMORAL ARTERY OF DEVELOPING PIGLETS
251. Aslak Steinsbekk: HOMEOPATHY IN THE PREVENTION OF UPPER RESPIRATORY TRACT INFECTIONS IN CHILDREN
252. Hill-Aina Steffenach: MEMORY IN HIPPOCAMPAL AND CORTICO-HIPPOCAMPAL CIRCUITS
253. Eystein Stordal: ASPECTS OF THE EPIDEMIOLOGY OF DEPRESSIONS BASED ON SELF-RATING IN A LARGE GENERAL HEALTH STUDY (THE HUNT-2 STUDY)
254. Viggo Pettersen: FROM MUSCLES TO SINGING: THE ACTIVITY OF ACCESSORY BREATHING MUSCLES AND THORAX MOVEMENT IN CLASSICAL SINGING
255. Marianne Fyhn: SPATIAL MAPS IN THE HIPPOCAMPUS AND ENTORHINAL CORTEX
256. Robert Valderhaug: OBSESSIVE-COMPULSIVE DISORDER AMONG CHILDREN AND ADOLESCENTS: CHARACTERISTICS AND PSYCHOLOGICAL MANAGEMENT OF PATIENTS IN OUTPATIENT PSYCHIATRIC CLINICS
257. Erik Skaaheim Haug: INFRARENAL ABDOMINAL AORTIC ANEURYSMS – COMORBIDITY AND RESULTS FOLLOWING OPEN SURGERY
258. Daniel Kondziella: GLIAL-NEURONAL INTERACTIONS IN EXPERIMENTAL BRAIN DISORDERS
259. Vegard Heimly Brun: ROUTES TO SPATIAL MEMORY IN HIPPOCAMPAL PLACE CELLS
260. Kenneth McMillan: PHYSIOLOGICAL ASSESSMENT AND TRAINING OF ENDURANCE AND STRENGTH IN PROFESSIONAL YOUTH SOCCER PLAYERS
261. Marit Sæbø Indredavik: MENTAL HEALTH AND CEREBRAL MAGNETIC RESONANCE IMAGING IN ADOLESCENTS WITH LOW BIRTH WEIGHT
262. Ole Johan Kemi: ON THE CELLULAR BASIS OF AEROBIC FITNESS, INTENSITY-DEPENDENCE AND TIME-COURSE OF CARDIOMYOCYTE AND ENDOTHELIAL ADAPTATIONS TO EXERCISE TRAINING
263. Eszter Vanky: POLYCYSTIC OVARY SYNDROME – METFORMIN TREATMENT IN PREGNANCY
264. Hild Fjærtoft: EXTENDED STROKE UNIT SERVICE AND EARLY SUPPORTED DISCHARGE. SHORT AND LONG-TERM EFFECTS
265. Grete Dyb: POSTTRAUMATIC STRESS REACTIONS IN CHILDREN AND ADOLESCENTS
266. Vidar Fykse: SOMATOSTATIN AND THE STOMACH
267. Kirsti Berg: OXIDATIVE STRESS AND THE ISCHEMIC HEART: A STUDY IN PATIENTS UNDERGOING CORONARY REVASCULARIZATION
268. Björn Inge Gustafsson: THE SEROTONIN PRODUCING ENTEROCHROMAFFIN CELL, AND EFFECTS OF HYPERSEROTONINEMIA ON HEART AND BONE

2006

269. Torstein Baade Rø: EFFECTS OF BONE MORPHOGENETIC PROTEINS, HEPATOCYTE GROWTH FACTOR AND INTERLEUKIN-21 IN MULTIPLE MYELOMA
270. May-Britt Tessem: METABOLIC EFFECTS OF ULTRAVIOLET RADIATION ON THE ANTERIOR PART OF THE EYE
271. Anne-Sofie Helvik: COPING AND EVERYDAY LIFE IN A POPULATION OF ADULTS WITH HEARING IMPAIRMENT
272. Therese Standal: MULTIPLE MYELOMA: THE INTERPLAY BETWEEN MALIGNANT PLASMA CELLS AND THE BONE MARROW MICROENVIRONMENT
273. Ingvild Saltvedt: TREATMENT OF ACUTELY SICK, FRAIL ELDERLY PATIENTS IN A GERIATRIC EVALUATION AND MANAGEMENT UNIT – RESULTS FROM A PROSPECTIVE RANDOMISED TRIAL
274. Birger Henning Endreseth: STRATEGIES IN RECTAL CANCER TREATMENT – FOCUS ON EARLY RECTAL CANCER AND THE INFLUENCE OF AGE ON PROGNOSIS
275. Anne Mari Aukan Rokstad: ALGINATE CAPSULES AS BIOREACTORS FOR CELL THERAPY
276. Mansour Akbari: HUMAN BASE EXCISION REPAIR FOR PRESERVATION OF GENOMIC STABILITY
277. Stein Sundstrøm: IMPROVING TREATMENT IN PATIENTS WITH LUNG CANCER – RESULTS FROM TWO MULITCENTRE RANDOMISED STUDIES
278. Hilde Pleym: BLEEDING AFTER CORONARY ARTERY BYPASS SURGERY - STUDIES ON HEMOSTATIC MECHANISMS, PROPHYLACTIC DRUG TREATMENT AND EFFECTS OF AUTOTRANSFUSION

279. Line Merethe Oldervoll: PHYSICAL ACTIVITY AND EXERCISE INTERVENTIONS IN CANCER PATIENTS
280. Boye Welde: THE SIGNIFICANCE OF ENDURANCE TRAINING, RESISTANCE TRAINING AND MOTIVATIONAL STYLES IN ATHLETIC PERFORMANCE AMONG ELITE JUNIOR CROSS-COUNTRY SKIERS
281. Per Olav Vandvik: IRRITABLE BOWEL SYNDROME IN NORWAY, STUDIES OF PREVALENCE, DIAGNOSIS AND CHARACTERISTICS IN GENERAL PRACTICE AND IN THE POPULATION
282. Idar Kirkeby-Garstad: CLINICAL PHYSIOLOGY OF EARLY MOBILIZATION AFTER CARDIAC SURGERY
283. Linn Getz: SUSTAINABLE AND RESPONSIBLE PREVENTIVE MEDICINE. CONCEPTUALISING ETHICAL DILEMMAS ARISING FROM CLINICAL IMPLEMENTATION OF ADVANCING MEDICAL TECHNOLOGY
284. Eva Tegnander: DETECTION OF CONGENITAL HEART DEFECTS IN A NON-SELECTED POPULATION OF 42,381 FETUSES
285. Kristin Gabestad Nørsett: GENE EXPRESSION STUDIES IN GASTROINTESTINAL PATHOPHYSIOLOGY AND NEOPLASIA
286. Per Magnus Haram: GENETIC VS. AQUIRED FITNESS: METABOLIC, VASCULAR AND CARDIOMYOCYTE ADAPTATIONS
287. Agneta Johansson: GENERAL RISK FACTORS FOR GAMBLING PROBLEMS AND THE PREVALENCE OG PATHOLOGICAL GAMBLING IN NORWAY
288. Svein Artur Jensen: THE PREVALENCE OF SYMPTOMATIC ARTERIAL DISEASE OF THE LOWER LIMB
289. Charlotte Björk Ingul: QUANITIFICATION OF REGIONAL MYOCARDIAL FUNCTION BY STRAIN RATE AND STRAIN FOR EVALUATION OF CORONARY ARTERY DISEASE. AUTOMATED VERSUS MANUAL ANALYSIS DURING ACUTE MYOCARDIAL INFARCTION AND DOBUTAMINE STRESS ECHOCARDIOGRAPHY
290. Jakob Nakling: RESULTS AND CONSEQUENCES OF ROUTINE ULTRASOUND SCREENING IN PREGNANCY – A GEOGRAPHIC BASED POPULATION STUDY
291. Anne Engum: DEPRESSION AND ANXIETY – THEIR RELATIONS TO THYROID DYSFUNCTION AND DIABETES IN A LARGE EPIDEMIOLOGICAL STUDY
292. Ottar Bjerkeset: ANXIETY AND DEPRESSION IN THE GENERAL POPULATION: RISK FACTORS, INTERVENTION AND OUTCOME – THE NORD-TRØNDELAG HEALTH STUDY (HUNT)
293. Jon Olav Drogset: RESULTS AFTER SURGICAL TREATMENT OF ANTERIOR CRUCIATE LIGAMENT INJURIES – A CLINICAL STUDY
294. Lars Fosse: MECHANICAL BEHAVIOUR OF COMPACTED MORSELLISED BONE – AN EXPERIMENTAL IN VITRO STUDY
295. Gunilla Klensmeden Fosse: MENTAL HEALTH OF PSYCHIATRIC OUTPATIENTS BULLIED IN CHILDHOOD
296. Paul Jarle Mork: MUSCLE ACTIVITY IN WORK AND LEISURE AND ITS ASSOCIATION TO MUSCULOSKELETAL PAIN
297. Björn Stenström: LESSONS FROM RODENTS: I: MECHANISMS OF OBESITY SURGERY – ROLE OF STOMACH. II: CARCINOGENIC EFFECTS OF *HELICOBACTER PYLORI* AND SNUS IN THE STOMACH

2007

298. Haakon R. Skogseth: INVASIVE PROPERTIES OF CANCER – A TREATMENT TARGET ? IN VITRO STUDIES IN HUMAN PROSTATE CANCER CELL LINES
299. Janniche Hammer: GLUTAMATE METABOLISM AND CYCLING IN MESIAL TEMPORAL LOBE EPILEPSY
300. May Britt Drugli: YOUNG CHILDREN TREATED BECAUSE OF ODD/CD: CONDUCT PROBLEMS AND SOCIAL COMPETENCIES IN DAY-CARE AND SCHOOL SETTINGS
301. Arne Skjold: MAGNETIC RESONANCE KINETICS OF MANGANESE DIPYRIDOXYL DIPHOSPHATE (MnDPDP) IN HUMAN MYOCARDIUM. STUDIES IN HEALTHY VOLUNTEERS AND IN PATIENTS WITH RECENT MYOCARDIAL INFARCTION
302. Siri Malm: LEFT VENTRICULAR SYSTOLIC FUNCTION AND MYOCARDIAL PERFUSION ASSESSED BY CONTRAST ECHOCARDIOGRAPHY
303. Valentina Maria do Rosario Cabral Iversen: MENTAL HEALTH AND PSYCHOLOGICAL ADAPTATION OF CLINICAL AND NON-CLINICAL MIGRANT GROUPS

304. Lasse Løvstakken: SIGNAL PROCESSING IN DIAGNOSTIC ULTRASOUND: ALGORITHMS FOR REAL-TIME ESTIMATION AND VISUALIZATION OF BLOOD FLOW VELOCITY
305. Elisabeth Olstad: GLUTAMATE AND GABA: MAJOR PLAYERS IN NEURONAL METABOLISM
306. Lilian Leistad: THE ROLE OF CYTOKINES AND PHOSPHOLIPASE A_2S IN ARTICULAR CARTILAGE CHONDROCYTES IN RHEUMATOID ARTHRITIS AND OSTEOARTHRITIS
307. Arne Vaaler: EFFECTS OF PSYCHIATRIC INTENSIVE CARE UNIT IN AN ACUTE PSYCIATHRIC WARD
308. Mathias Toft: GENETIC STUDIES OF LRRK2 AND PINK1 IN PARKINSON'S DISEASE
309. Ingrid Løvold Mostad: IMPACT OF DIETARY FAT QUANTITY AND QUALITY IN TYPE 2 DIABETES WITH EMPHASIS ON MARINE N-3 FATTY ACIDS
310. Torill Eidhammer Sjøbakk: MR DETERMINED BRAIN METABOLIC PATTERN IN PATIENTS WITH BRAIN METASTASES AND ADOLESCENTS WITH LOW BIRTH WEIGHT
311. Vidar Beisvåg: PHYSIOLOGICAL GENOMICS OF HEART FAILURE: FROM TECHNOLOGY TO PHYSIOLOGY
312. Olav Magnus Søndenå Fredheim: HEALTH RELATED QUALITY OF LIFE ASSESSMENT AND ASPECTS OF THE CLINICAL PHARMACOLOGY OF METHADONE IN PATIENTS WITH CHRONIC NON-MALIGNANT PAIN
313. Anne Brantberg: FETAL AND PERINATAL IMPLICATIONS OF ANOMALIES IN THE GASTROINTESTINAL TRACT AND THE ABDOMINAL WALL
314. Erik Solligård: GUT LUMINAL MICRODIALYSIS
315. Elin Tollefsen: RESPIRATORY SYMPTOMS IN A COMPREHENSIVE POPULATION BASED STUDY AMONG ADOLESCENTS 13-19 YEARS. YOUNG-HUNT 1995-97 AND 2000-01; THE NORD-TRØNDELAG HEALTH STUDIES (HUNT)
316. Anne-Tove Brenne: GROWTH REGULATION OF MYELOMA CELLS
317. Heidi Knobel: FATIGUE IN CANCER TREATMENT – ASSESSMENT, COURSE AND ETIOLOGY
318. Torbjørn Dahl: CAROTID ARTERY STENOSIS. DIAGNOSTIC AND THERAPEUTIC ASPECTS
319. Inge-Andre Rasmussen jr.: FUNCTIONAL AND DIFFUSION TENSOR MAGNETIC RESONANCE IMAGING IN NEUROSURGICAL PATIENTS
320. Grete Helen Bratberg: PUBERTAL TIMING – ANTECEDENT TO RISK OR RESILIENCE ? EPIDEMIOLOGICAL STUDIES ON GROWTH, MATURATION AND HEALTH RISK BEHAVIOURS; THE YOUNG HUNT STUDY, NORD-TRØNDELAG, NORWAY
321. Sveinung Sørhaug: THE PULMONARY NEUROENDOCRINE SYSTEM. PHYSIOLOGICAL, PATHOLOGICAL AND TUMOURIGENIC ASPECTS
322. Olav Sande Eftedal: ULTRASONIC DETECTION OF DECOMPRESSION INDUCED VASCULAR MICROBUBBLES
323. Rune Bang Leistad: PAIN, AUTONOMIC ACTIVATION AND MUSCULAR ACTIVITY RELATED TO EXPERIMENTALLY-INDUCED COGNITIVE STRESS IN HEADACHE PATIENTS
324. Svein Brekke: TECHNIQUES FOR ENHANCEMENT OF TEMPORAL RESOLUTION IN THREE-DIMENSIONAL ECHOCARDIOGRAPHY
325. Kristian Bernhard Nilsen: AUTONOMIC ACTIVATION AND MUSCLE ACTIVITY IN RELATION TO MUSCULOSKELETAL PAIN
326. Anne Irene Hagen: HEREDITARY BREAST CANCER IN NORWAY. DETECTION AND PROGNOSIS OF BREAST CANCER IN FAMILIES WITH *BRCA1*GENE MUTATION
327. Ingebjørg S. Juel : INTESTINAL INJURY AND RECOVERY AFTER ISCHEMIA. AN EXPERIMENTAL STUDY ON RESTITUTION OF THE SURFACE EPITHELIUM, INTESTINAL PERMEABILITY, AND RELEASE OF BIOMARKERS FROM THE MUCOSA
328. Runa Heimstad: POST-TERM PREGNANCY
329. Jan Egil Afset: ROLE OF ENTEROPATHOGENIC *ESCHERICHIA COLI* IN CHILDHOOD DIARRHOEA IN NORWAY
330. Bent Håvard Hellum: *IN VITRO* INTERACTIONS BETWEEN MEDICINAL DRUGS AND HERBS ON CYTOCHROME P-450 METABOLISM AND P-GLYCOPROTEIN TRANSPORT
331. Morten André Høydal: CARDIAC DYSFUNCTION AND MAXIMAL OXYGEN UPTAKE MYOCARDIAL ADAPTATION TO ENDURANCE TRAINING

2008

332. Andreas Møllerløkken: REDUCTION OF VASCULAR BUBBLES: METHODS TO PREVENT THE ADVERSE EFFECTS OF DECOMPRESSION
333. Anne Hege Aamodt: COMORBIDITY OF HEADACHE AND MIGRAINE IN THE NORD-TRØNDELAG HEALTH STUDY 1995-97
334. Brage Høyem Amundsen: MYOCARDIAL FUNCTION QUANTIFIED BY SPECKLE TRACKING AND TISSUE DOPPLER ECHOCARDIOGRAPHY – VALIDATION AND APPLICATION IN EXERCISE TESTING AND TRAINING
335. Inger Anne Næss: INCIDENCE, MORTALITY AND RISK FACTORS OF FIRST VENOUS THROMBOSIS IN A GENERAL POPULATION. RESULTS FROM THE SECOND NORD-TRØNDELAG HEALTH STUDY (HUNT2)
336. Vegard Bugten: EFFECTS OF POSTOPERATIVE MEASURES AFTER FUNCTIONAL ENDOSCOPIC SINUS SURGERY
337. Morten Bruvold: MANGANESE AND WATER IN CARDIAC MAGNETIC RESONANCE IMAGING
338. Miroslav Fris: THE EFFECT OF SINGLE AND REPEATED ULTRAVIOLET RADIATION ON THE ANTERIOR SEGMENT OF THE RABBIT EYE
339. Svein Arne Aase: METHODS FOR IMPROVING QUALITY AND EFFICIENCY IN QUANTITATIVE ECHOCARDIOGRAPHY – ASPECTS OF USING HIGH FRAME RATE
340. Roger Almvik: ASSESSING THE RISK OF VIOLENCE: DEVELOPMENT AND VALIDATION OF THE BRØSET VIOLENCE CHECKLIST
341. Ottar Sundheim: STRUCTURE-FUNCTION ANALYSIS OF HUMAN ENZYMES INITIATING NUCLEOBASE REPAIR IN DNA AND RNA
342. Anne Mari Undheim: SHORT AND LONG-TERM OUTCOME OF EMOTIONAL AND BEHAVIOURAL PROBLEMS IN YOUNG ADOLESCENTS WITH AND WITHOUT READING DIFFICULTIES
343. Helge Garåsen: THE TRONDHEIM MODEL. IMPROVING THE PROFESSIONAL COMMUNICATION BETWEEN THE VARIOUS LEVELS OF HEALTH CARE SERVICES AND IMPLEMENTATION OF INTERMEDIATE CARE AT A COMMUNITY HOSPITAL COULD PROVIDE BETTER CARE FOR OLDER PATIENTS. SHORT AND LONG TERM EFFECTS
344. Olav A. Foss: "THE ROTATION RATIOS METHOD". A METHOD TO DESCRIBE ALTERED SPATIAL ORIENTATION IN SEQUENTIAL RADIOGRAPHS FROM ONE PELVIS
345. Bjørn Olav Åsvold: THYROID FUNCTION AND CARDIOVASCULAR HEALTH
346. Torun Margareta Melø: NEURONAL GLIAL INTERACTIONS IN EPILEPSY
347. Irina Poliakova Eide: FETAL GROWTH RESTRICTION AND PRE-ECLAMPSIA: SOME CHARACTERISTICS OF FETO-MATERNAL INTERACTIONS IN DECIDUA BASALIS
348. Torunn Askim: RECOVERY AFTER STROKE. ASSESSMENT AND TREATMENT; WITH FOCUS ON MOTOR FUNCTION
349. Ann Elisabeth Åsberg: NEUTROPHIL ACTIVATION IN A ROLLER PUMP MODEL OF CARDIOPULMONARY BYPASS. INFLUENCE ON BIOMATERIAL, PLATELETS AND COMPLEMENT
350. Lars Hagen: REGULATION OF DNA BASE EXCISION REPAIR BY PROTEIN INTERACTIONS AND POST TRANSLATIONAL MODIFICATIONS
351. Sigrun Beate Kjøtrød: POLYCYSTIC OVARY SYNDROME – METFORMIN TREATMENT IN ASSISTED REPRODUCTION
352. Steven Keita Nishiyama: PERSPECTIVES ON LIMB-VASCULAR HETEROGENEITY: IMPLICATIONS FOR HUMAN AGING, SEX, AND EXERCISE
353. Sven Peter Näsholm: ULTRASOUND BEAMS FOR ENHANCED IMAGE QUALITY
354. Jon Ståle Ritland: PRIMARY OPEN-ANGLE GLAUCOMA & EXFOLIATIVE GLAUCOMA. SURVIVAL, COMORBIDITY AND GENETICS
355. Sigrid Botne Sando: ALZHEIMER'S DISEASE IN CENTRAL NORWAY. GENETIC AND EDUCATIONAL ASPECTS
356. Parvinder Kaur: CELLULAR AND MOLECULAR MECHANISMS BEHIND METHYLMERCURY-INDUCED NEUROTOXICITY
357. Ismail Cüneyt Güzey: DOPAMINE AND SEROTONIN RECEPTOR AND TRANSPORTER GENE POLYMORPHISMS AND EXTRAPYRAMIDAL SYMPTOMS. STUDIES IN PARKINSON'S DISEASE AND IN PATIENTS TREATED WITH ANTIPSYCHOTIC OR ANTIDEPRESSANT DRUGS

358. Brit Dybdahl: EXTRA-CELLULAR INDUCIBLE HEAT-SHOCK PROTEIN 70 (Hsp70) – A ROLE IN THE INFLAMMATORY RESPONSE ?
359. Kristoffer Haugarvoll: IDENTIFYING GENETIC CAUSES OF PARKINSON'S DISEASE IN NORWAY
360. Nadra Nilsen: TOLL.LIKE RECEPTOR – EXPRESSION, REGULATION AND SIGNALING
361. Johan Håkon Bjørngaard: PATIENT SATISFACTION WITH OUTPATIENT MENTAL HEALTH SERVICES – THE INFLUENCE OF ORGANIZATIONAL FACTORS.
362. Kjetil Høydal : EFFECTS OF HIGH INTENSITY AEROBIC TRAINING IN HEALTHY SUBJECTS AND CORONARY ARTERY DISEASE PATIENTS; THE IMPORTANCE OF INTENSITY,, DURATION AND FREQUENCY OF TRAINING.
363. Trine Karlsen: TRAINING IS MEDICINE: ENDURANCE3 AND STRANGTH TRAINING IN CORONARY ARTERY DISESE AND HEALTH.
364. Marte Thuen: MANGANASE-ENHANCED AND DIFFUSION TENSOR MR IMAGING OF THE NORMAL, INJURED AND REGENERATING RAT VISUAL PATHWAY.